INL/EXT-13-28842

Results of U-xMo (x=7, 10, 12 wt.%) Alloy Versus Al-6061 Cladding Diffusion Couple Experiments Performed at 500, 550 and 600°C

Emmanuel Perez
Dennis D. Keiser, Jr.
Yongho Sohn

April 2013

The INL is a U.S. Department of Energy National Laboratory
operated by Battelle Energy Alliance

INL/EXT-13-28842

Results of U-xMo (x=7, 10, 12 wt.%) Alloy Versus Al-6061 Cladding Diffusion Couple Experiments Performed at 500, 550 and 600°C

Emmanuel Perez
Dennis D. Keiser, Jr.
Yongho Sohn[1]

[1]University of Central Florida

April 2013

Idaho National Laboratory
Idaho Falls, Idaho 83415

http://www.inl.gov

Prepared for the
U.S. Department of Energy
Office of National Nuclear Security Administration
Under DOE Idaho Operations Office
Contract DE-AC07-05ID14517

ABSTRACT

The Reduced Enrichment for Research and Test Reactors (RERTR) program has been developing low-enrichment fuel systems encased in Al-6061 for use in research and test reactors. U–Mo alloys in contact with Al and Al alloys can undergo diffusional interactions that can result in the development of interdiffusion zones with complex fine-grained microstructures composed of multiple phases. A monolithic fuel currently being developed by the RERTR program has local regions where the U–Mo fuel plate is in contact with the Al-6061 cladding and, as a result, the program finds information about interdiffusion zone development at high temperatures of interest. In this study, the microstructural development of diffusion couples consisting of U-7wt.%Mo, U-10wt.%Mo, and U-12wt.%Mo vs. Al-6061 (or 6061 aluminum) cladding, annealed at 500, 550, 600°C for 1, 5, 20, 24, or 132 hours, was analyzed by backscatter electron microscopy and x-ray energy dispersive spectroscopy on a scanning electron microscope. Concentration profiles were determined by standardized wavelength dispersive spectroscopy and standardless x-ray energy dispersive spectroscopy. The results of this work shows that the presence of surface layers at the U–Mo/Al-6061 interface can dramatically impact the overall interdiffusion behavior in terms of rate of interaction and uniformity of the developed interdiffusion zones. It further reveals that relatively uniform interaction layers with higher Si concentrations can develop in U–Mo/Al-6061 couples annealed at shorter times and that longer times at temperature result in the development of more non-uniform interaction layers with more areas that are enriched in Al. At longer annealing times and relatively high temperatures, U–Mo/Al-6061 couples can exhibit more interaction compared to U–Mo/pure Al couples. The minor alloying constituents in Al-6061 cladding can result in the development of many complex phases in the interaction layer of U–Mo/Al–6061 cladding couples, and some phases in the interdiffusion zones of U–Mo/Al–6061 cladding couples are likely similar to those observed for U–Mo/pure Al couples.

CONTENTS

FIGURES

TABLES

ACRONYMS

DU	depleted uranium
EPMA	electron probe microanalysis
FE-SEM	field-emission scanning electron microscopy
PFZ	precipitate-free zone
SE	secondary electron
SEM	scanning electron microscopy
TTT	time temperature transformation
WDS	wavelength dispersive spectroscopy
EDS	x-ray energy dispersive spectroscopy

RESULTS OF U-XMO (X=7, 10, 12 WT.%) ALLOY VERSUS AL-6061 CLADDING DIFFUSION COUPLE EXPERIMENTS PERFORMED AT 500, 550 AND 600°C

1. INTRODUCTION

Diffusional interactions in the U–Mo-Al system have been extensively studied through diffusion-couple experiments [1-8], alloy casting and characterization [9, 10], and characterization of U–Mo dispersions in Al matrix and monolithic plate assemblies encased in Al alloy [4, 5, 11-18]. The studies have been carried out to support the Reduced Enrichment for Research and Test Reactors (RERTR) program [13] for the development of low-enriched U–Mo fuels encased in Al [13, 19-21]. In U–Mo fuel alloys, alloying U with Mo stabilizes the (bcc) γ-U phase. Mo has high solubility in γ-U that allows for fuel customization, and the alloy satisfies the fissile-U densities required by the RERTR program. Extensive studies and characterization of U–Mo alloys have been carried out to develop an understanding of the phase equilibria [22-44], kinetics [45-52], mechanical properties [53-57], thermodynamics [58-62] and irradiation behavior [63-73] of this system. In early studies, Pfeil [22], Saller et al. [23-25], Ivanov et al. [29, 34], Carrera et al. [26] and Dwight et al.[27] detailed the γ-U→(α-U + δ-U_2Mo) decomposition that takes place below 573°C. Howlett et al. [48] and Repas et al. [50] developed time-temperature-transformation (TTT) diagrams for U–Mo alloys ranging from 2.5 to 14 wt.% Mo.

The U–Mo alloys in contact with Al undergo complex diffusional interactions that can produce various phases with undesirable growth kinetics [1-8 11-18] and irradiation behavior [67-71, 73, 75-79]. In a prior study by the authors [7,8], U–Mo alloys and high purity Al (99.999%) were used to assemble diffusion couples, and UAl_3, UAl_4, $U_6Mo_4Al_{43}$ and UMo_2Al_{20} phases were observed to develop in the interaction region. The number of phases that developed in the interaction region was analyzed with respect to the number of components and the thermodynamic degrees of freedom available for the system.

In dispersion and monolithic fuels, Al–6061 (aluminum 6061 alloy) is used as a cladding to encase the U–Mo fuel to provide structural stability and to isolate the fuel. For monolithic fuel plates, interactions between the U–Mo and the Al–6061 can take place in localized areas at high temperature during fuel plate manufacture, and in reactor primarily due to irradiation. The nominal composition of the Al–6061, in wt%, is Al-1.0Mg-0.6Si-0.7Fe-0.25Zn-0.2Cu-0.2Cr-0.15Mn-0.15Ti. The number of alloying additions increases the available thermodynamic degrees of freedom which allows for the possibility for the development of several different phases.

In this study, phase constituents and growth of the interaction layers that develop between U–Mo alloys and Al–6061 were examined using solid-to-solid diffusion couples assembled with U-7wt.%Mo, U-10wt.%Mo and U-12wt.%Mo in contact with Al–6061. The couples were annealed at 500, 550, 600°C for 1, 5, 20, 24, or 132 hours. Interaction layer thickness, phase compositions and concentration profiles were examined by scanning electron microscopy (SEM) and energy dispersive x-ray spectroscopy (EDS). Concentration profiles were also generated by electron probe microanalysis collected through standardized wavelength dispersive spectroscopy (WDS),

and from these profiles, interdiffusion flux profiles were calculated for selected couples. From the interdiffusion flux profiles, the integrated interdiffusion coefficients (e.g., accumulative interdiffusion fluxes) of U, Mo, and Al were selectively determined.

2. EXPERIMENTAL

2.1 Compositional and Microstructural Characterization of U–Mo Alloys

The U–7Mo, U–10Mo and U–12Mo alloys were cast using high-purity depleted uranium (DU) and Mo via arc-melting. Each was melted three times to ensure homogeneity and then drop-cast to form rods. The as-cast rods were homogenized in an Ar atmosphere at 950°C for 96 hours. The U–Mo alloys were water-quenched in ice water after homogenization to retain the high-temperature γ-phase. Disks, 0.64 cm diameter and 2-3mm in thickness, were sectioned from the homogenized U–7Mo, U–10Mo and U–12Mo alloy rods. Each disk was individually epoxy-mounted and metallographically polished down to 1μm. The alloy compositions were determined by electron probe microanalysis (EPMA) using pure elemental standards. The composition at five randomly chosen locations was measured and averaged. The microstructures and compositions of these alloys were also examined by using field-emission scanning electron microscopy (FE-SEM) with EDS, and by x-ray diffraction (XRD) using a Rigaku XRD system operated at 40Kv and 30mA.

2.2 Diffusion Couple Annealing and Characterization

All the couples were assembled under a controlled Ar atmosphere to prevent or minimize the formation of oxide scale that may interfere with interdiffusion. Alloys for diffusion couples were sectioned into disks, 0.64 cm diameter by 2-3 mm in thickness for the DU alloys and 6 mm in thickness for the Al–6061. The surfaces of the disks were metallographically polished manually to 600-grit using abrasive grinding paper. The final polishing step was carried out using 1μm diamond paste.

Initially, diffusion couples were assembled and annealed using samples that were only polished (Table I), where sample surfaces were polished with 1 μm diamond paste for several minutes to remove any oxide that may have developed over time. The surfaces were then cleaned with soap and water and dried with Ar gas. The diffusion couples were assembled immediately thereafter. The polished surfaces were placed in contact with each other and held together by two clamping disks with rods made of steel to form a jig.

To determine whether the optimal method for sample surface preparation for diffusion couple experiments should include nitric acid treatment, an experiment was carried out to determine whether this treatment would help remove the oxide layer that is normally present on the alloy surface. For Al alloys, nitric acid dissolves the Al_2O_3 oxide layer that forms naturally on the alloy. The same acid has been used in other diffusion experiments [80] to remove the oxide from uranium alloy. Both the uranium and aluminum were first immersed in concentrated nitric acid for from 30 seconds to one minute. After the alloys were acid treated, they were cleaned with soap, water, and ethanol. The Al alloys were not further polished. The uranium alloys were repolished to remove the observed oxide scale that developed and were not further acid treated.

The diffusion couples were assembled in the same fashion mentioned above. Based on the results of this study, a set of diffusion couples were annealed and characterized using the nitric acid treatment only on the Al–6061 samples (see Table II).

Table I. Diffusion couples between Al–6061 cladding and U–7Mo, U–10Mo and U–12Mo alloys annealed at 500, 550, and 600°C (polishing only).

Temperature	U–Mo Alloy	Al-alloy	Time of Anneal (h)
600°C	U-7wt.%Mo	6061	24
	U-10wt.%Mo	6061	24
	U-12wt.%Mo	6061	24
550°C	U-7wt.%Mo	6061	24
	U-10wt.%Mo	6061	24
	U-12wt.%Mo	6061	24
500°C	U-7wt.%Mo	6061	132
	U-10wt.%Mo	6061	132
	U-12wt.%Mo	6061	132

Table II. Diffusion couples between Al–6061 cladding and U–7Mo, U–10Mo and U–12Mo alloys annealed at 550 and 600°C (nitric acid treatment of Al–6061).

Temperature	U–Mo Alloy	Al-alloy	Time of Anneal (h)
600°C	U-7wt.%Mo	6061	24
	U-10wt.%Mo	6061	24
	U-12wt.%Mo	6061	24
550°C	U-7wt.%Mo	6061	1
550°C	U-7wt.%Mo	6061	5
	U-10wt.%Mo	6061	5
	U-12wt.%Mo	6061	5
550°C	U-7wt.%Mo	6061	20
	U-10wt.%Mo	6061	20
	U-12wt.%Mo	6061	20

For all diffusion couples, the jig assembly was placed in quartz capsules. Ta foil was placed in the capsules to serve as an oxygen trap. The capsules were then sealed on one end, evacuated to 1×10^{-6} torr, and purged with hydrogen. Hydrogen purging and evacuation was repeated several times before each capsule was finally filled with ultra high purity argon. The final argon pressure in the capsule was controlled so that the pressure inside the capsule was approximately one atmosphere at the annealing temperature. The capsules were then sealed and placed at the center of a Lindberg/Blue three-zone tube

furnace, maintained at diffusion anneal temperature. The furnace ends were fully insulated to minimize temperature gradients.

After diffusion annealing, the diffusion couples were quenched by breaking the quartz capsule in ice water. Each diffusion couple was then mounted in epoxy, and metallographically prepared for microstructural observations by SEM/EDS and compositional analysis by EPMA. Experimental concentration profiles for the diffusion couples were determined by EPMA (JEOL 733 Superprobe) equipped with four detectors. Pure Al, Mo, Si, Mg and UO_2 were used as pure standards. Point-to-point counting technique (Δx ~10μm) was employed for the measurements. Experimental concentration profiles were smoothed using Matlab's spline interpolation tool for quantitative analysis.

3. RESULTS

3.1 Microstructural Features Observed for Diffusion Couples Prepared Using Polishing Alone

3.1.1 Diffusion Couples Annealed at 600°C for 24 Hours

The diffusion couples, U–7Mo vs. Al–6061, U–10Mo vs. Al–6061, and U–12Mo vs. Al–6061, developed significant interdiffusion zones after 24 hours of anneal at 600°C, as presented in Figure 1 through Figure 3. The interdiffusion zones between all the U–Mo and Al–6061 produced an Al-rich phase, tentatively identified by an average composition sumarized as $(U,Mo)Al_4$ phase. Note that based on backscatter contrast the interdiffusion zones are composed of several phases. Based on backscatter electron images, the thickness of the Al-rich intermetallic phase of each diffusion couple was measured and reported in Table III. In addition to the measurements from the backscatter electron photomicrographs, additional determination of intermetallic thickness was carried out from concentration profiles determined by EPMA. The results from these measurements are reported in Table IV. Although this data represent one section within the diffusion zone, relative consistency in the measured thickness can be found between Table III and Table IV. The growth rate of the intermetallic phase region can be considered relatively large for this Al–6061 alloy, which contains low Si (0.4 ~ 0.8 wt. %) and Mg (0.8 ~ 1.2 wt. %) concentrations.

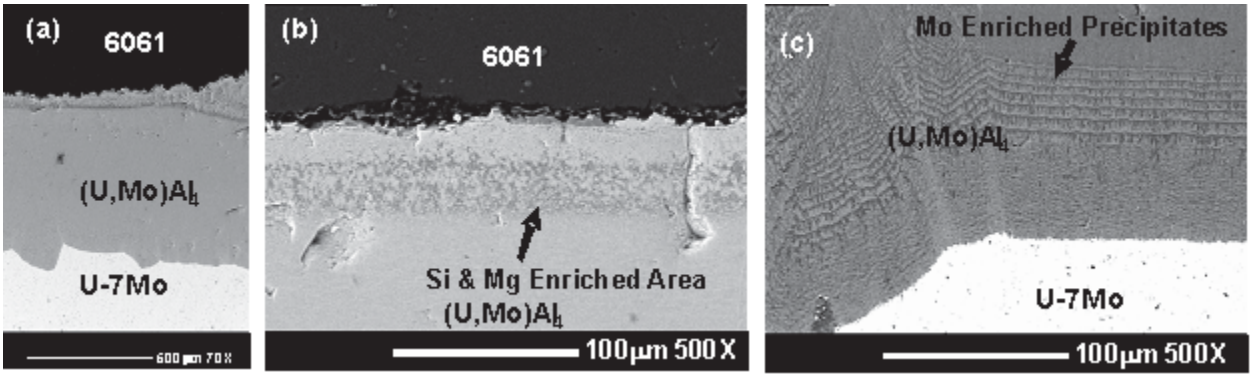

Figure 1. Backscatter electron micrographs of the U–7Mo vs. Al–6061 diffusion couple annealed at 600°C for 24 hours showing: (a) the entire interdiffusion zone containing, tentatively identified by composition, $(U,Mo)Al_4$, (b) the Al-rich and (c) the U–Mo-rich side of the $(U,Mo)Al_4$ composition region.

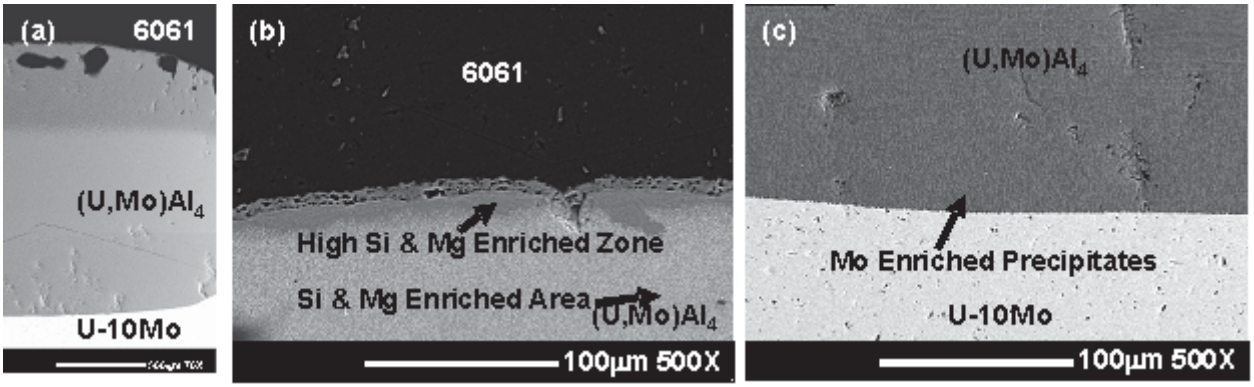

Figure 2. Backscatter electron micrographs of the U–10Mo vs. Al–6061 diffusion couple annealed at 600°C for 24 hours showing: (a) the entire interdiffusion zone containing, tentatively identified by composition, $(U,Mo)Al_4$, (b) the Al-rich and (c) the U–Mo-rich side of the $(U,Mo)Al_4$ composition region.

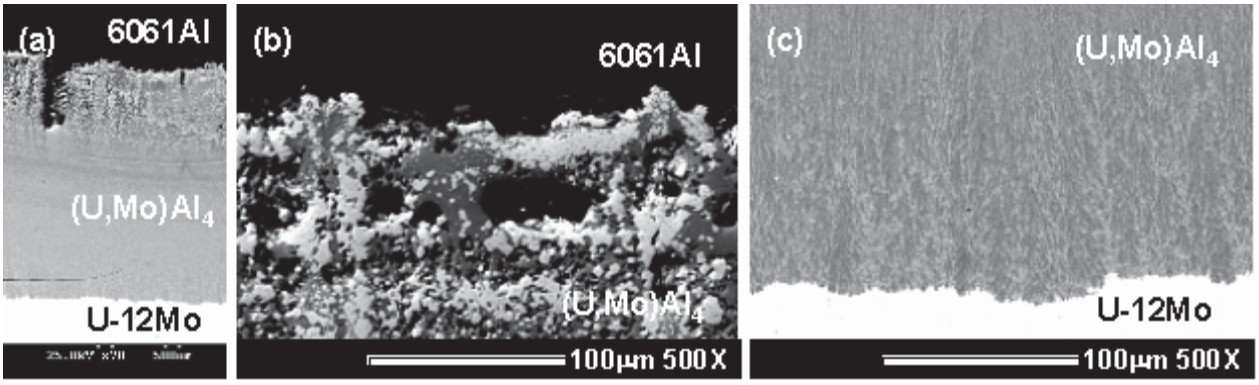

Figure 3. Backscatter electron micrographs of the U–12Mo vs. Al–6061Al diffusion couple annealed at 600°C for 24 hours showing: (a) the entire interdiffusion zone containing, tentatively identified by composition, $(U,Mo)Al_4$, (b) the Al-rich and (c) the U–Mo-rich side of the $(U,Mo)Al_4$ composition region.

Table III. Interdiffusion zone thickness measured from backscatter electron photomicrographs.

Diffusion Couple	U–7Mo vs. Al–6061	U–10Mo vs. Al–6061	U–12Mo vs. Al–6061
Thickness (µm)	658	1550	925

Table IV. Interdiffusion zone thickness determined by the measured EPMA concentration profiles.

Diffusion Couple	U–7Mo vs. Al–6061	U–10Mo vs. Al–6061	U–12Mo vs. Al–6061
Thickness (µm)	720	1430	820

3.1.1.1 Concentration Profiles, Interdiffusion Fluxes and Integrated Interdiffusion Coefficients from Couples Annealed at 600°C for 24 Hours

The interdiffusion fluxes of individual components may be determined directly from their concentration profiles by:[81]

$$\tilde{J} = \frac{1}{2t}\int_{C_i^{\pm\infty}}^{C_i(x)} (x - x_o)dC_i \qquad (i = 1,2,\dots,n)$$

where $\tilde{J}$ is the interdiffusion flux of component i in an n component system, t is the diffusion anneal time and C_i is the concentration of component i. The profile of interdiffusion flux for a component can be integrated with respect to distance, and this accumulated interdiffusion flux for a component can be defined as integrated interdiffusion coefficients, $D_{i,\Delta x}^{int}$ over a selected region, x_1 from x_2, as:

$$D_{i,\Delta x}^{int} = \int_{x_1}^{x_2} \tilde{J}_i dx$$

The experimental concentration profiles, after smoothing, were employed to determine interdiffusion fluxes of major components, namely U, Mo and Al, as presented in Figure 4 (b) through Figure 6 (b) for U–7Mo vs. Al–6061, U–10Mo vs. Al–6061 and U–12Mo vs. Al–6061 couples, respectively. From the interdiffusion flux profiles, the integrated interdiffusion coefficients (e.g., accumulative interdiffusion fluxes) of U, Mo and Al were determined and are reported in Table V.

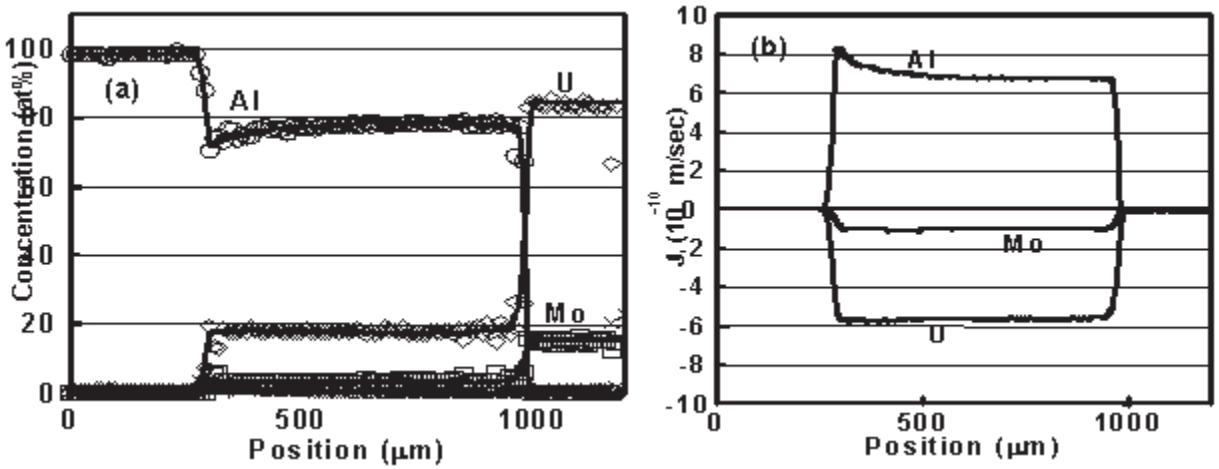

Figure 4. (a) Concentration profiles and (b) corresponding interdiffusion flux profiles from U–7Mo vs. Al–6061 diffusion couple annealed at 600°C for 24 hours.

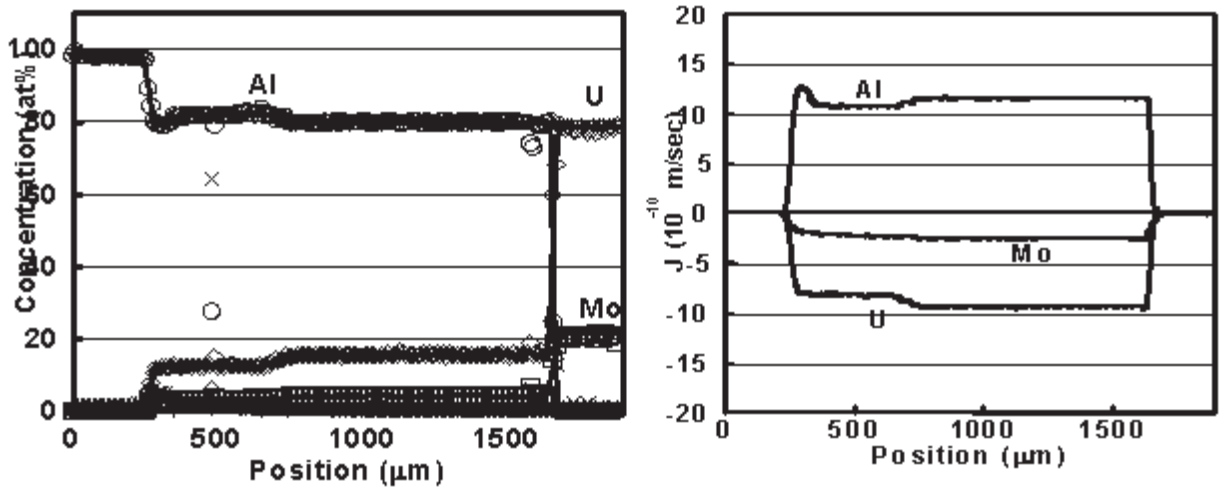

Figure 5. (a) Concentration profiles and (b) corresponding interdiffusion flux profiles from U–10Mo vs. Al–6061 diffusion couple annealed at 600°C for 24 hours.

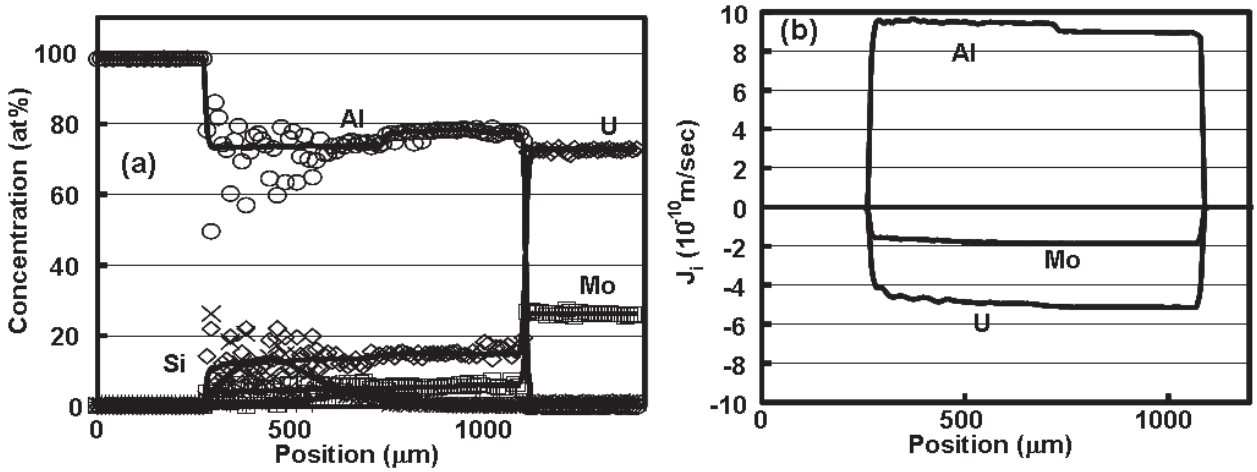

Figure 6. (a) Concentration profiles and (b) corresponding interdiffusion flux profiles from U–12Mo vs. Al–6061 diffusion couple annealed at 600°C for 24 hours.

Table V. Integrated interdiffusion coefficients $D_{t,\Delta x}^{int}$ of Al, Mo and U in the diffusion couples treated at 600°C for 24 hours. These integrated interdiffusion coefficients largely represent cumulative interdiffusion fluxes across the intermetallic phase region.

Diffusion Couple	$D_{t,\Delta x}^{int}$ (10^{-14} m^2/sec)		
	U	Mo	Al
U–7Mo vs. Al–6061	-40.20	-7.36	49.90
U–10Mo vs. Al–6061	-126.00	-34.10	161.00
U–12Mo vs. Al–6061	-48.3	-17.69	75.00

Si, Mg, and Mo concentrations have been highlighted in the concentration profiles for U–7Mo vs. Al–6061, U–10Mo vs. Al–6061 and U–12Mo vs. Al–6061 (see Figure 7 through Figure 9). These profiles

show some scatter in the data due to the fine mixture in the multi-phase regions near the U–Mo/intermetallic and intermetallic/Al-alloy interfaces, as shown in backscatter micrographs from Figure 1 through Figure 3. Accumulations of Mg and Si are observed near the intermetallic/Al-alloy interfaces in Figure 7 and Figure 8 for the U–7Mo and U–10Mo vs. Al–6061 couples, respectively. The U–12Mo vs. Al–6061 couple experienced a higher Si buildup than the couples with U–7Mo and U–10Mo, as can be observed in Figure 9. This may support silicide formation in the presence of Mo. It also explains the apparent discrepancy in the $D^{inp}_{i,\Delta x}$ shown in Table V above. When the $D^{inp}_{i,\Delta x}$ for Si and Mg are included, the sum of the coefficients adds to zero, as expected.

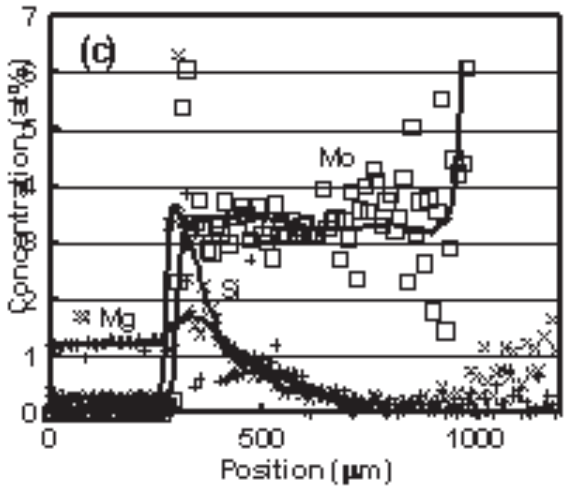

Figure 7. Detailed Si, Mg, and Mo concentration profiles from the U–7Mo vs. Al–6061 diffusion couple annealed at 600°C for 24 hours.

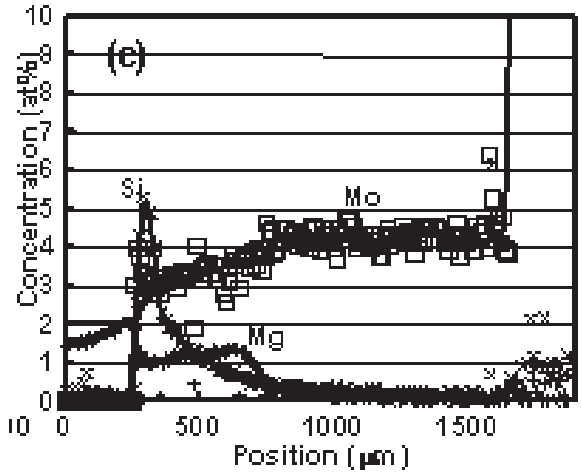

Figure 8. Detailed Si, Mg, and Mo concentration profiles from the U–10Mo vs. Al–6061 diffusion couple annealed at 600°C for 24 hours.

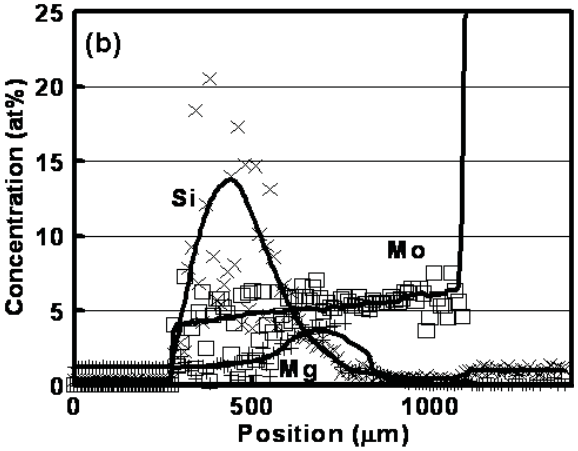

Figure 9. Detailed Si, Mg, and Mo concentration profiles from the U–12Mo vs. Al–6061 diffusion couple annealed at 600°C for 24 hours.

3.1.2 Diffusion Couples Annealed at 550°C for 24 Hours

Diffusion couples of U–7Mo, U–10Mo and U–12Mo vs. Al–6061 were assembled and annealed at 550°C for 24 hours. Microstructural and compositional analyses were carried out for these couples. The developed interdiffusion zones for the couples treated at 550°C for 24 hours were significantly smaller than those treated at 600°C for the same treatment time. Figure 10 through Figure 12 show backscatter electron micrographs of the diffusion couples with detailed micrographs showing the interfaces between the Al alloy and the intermetallic phase, and the interface between the U–Mo alloy and intermetallic phase.

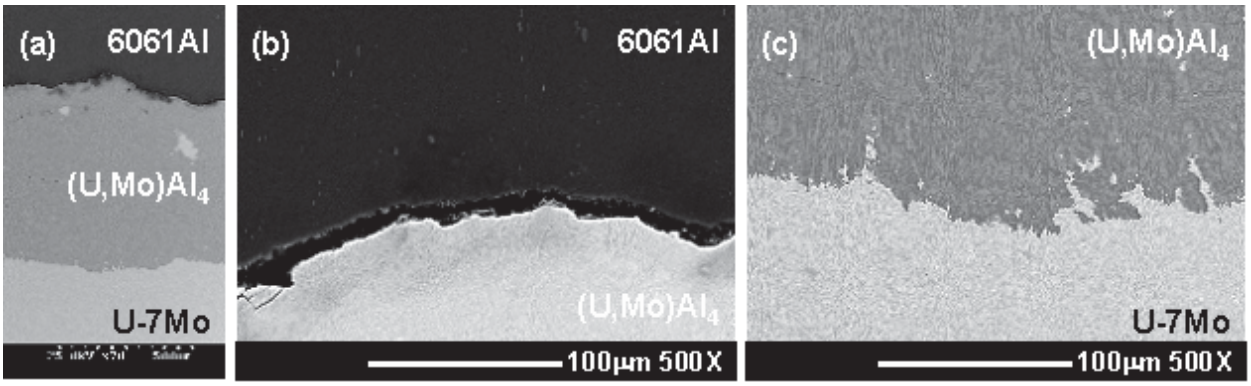

Figure 10. Backscatter electron micrographs of the U–7Mo vs. Al–6061 diffusion couple annealed at 550°C for 24 hours: showing (a) the entire interdiffusion zone containing, tentatively identified by composition, $(U,Mo)Al_4$, (b) the Al-rich and (c) the U–Mo-rich side of the $(U,Mo)Al_4$ composition region.

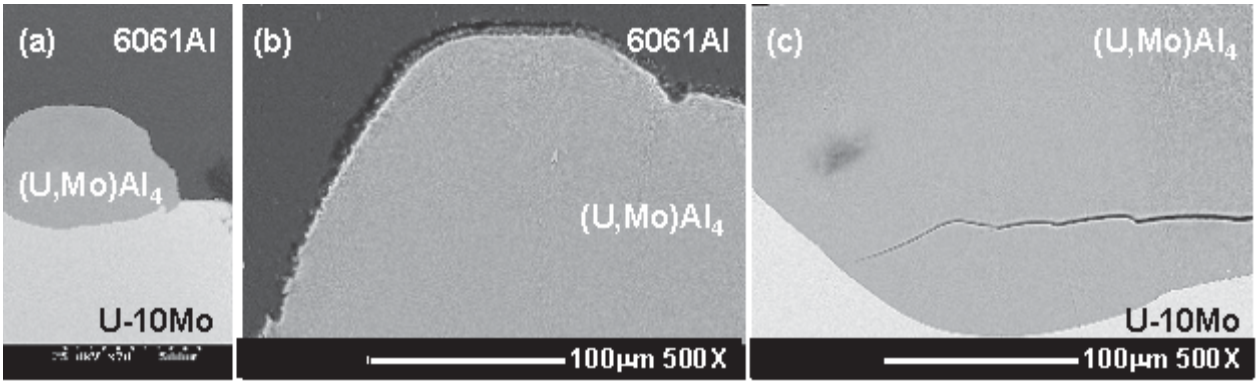

Figure 11. Backscatter electron micrographs of the U–10Mo vs. Al–6061 diffusion couple annealed at 550°C for 24 hours: showing (a) the entire interdiffusion zone containing, tentatively identified by composition, $(U,Mo)Al_4$, (b) the Al-rich and (c) the U–Mo-rich side of the $(U,Mo)Al_4$ composition region.

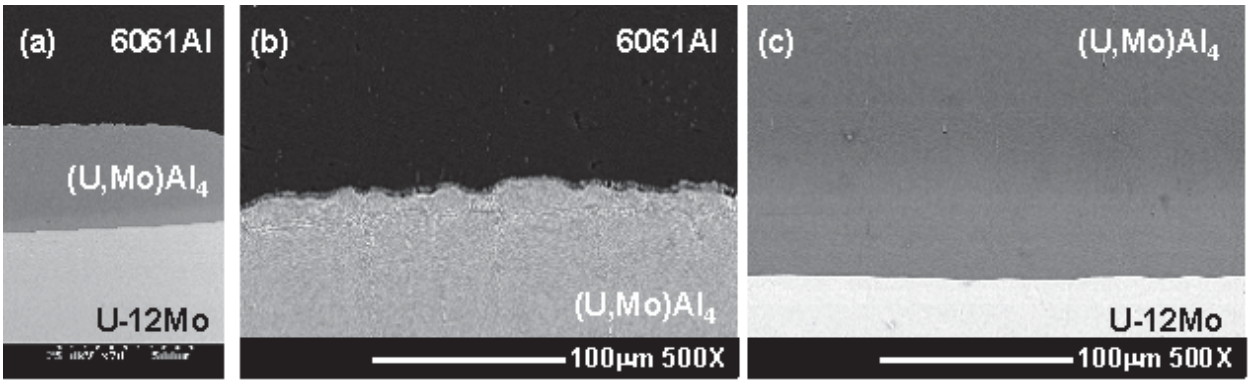

Figure 12. Backscatter electron micrographs of the U–12Mo vs. Al–6061 diffusion couple annealed at 550°C for 24 hours: showing (a) the entire interdiffusion zone containing, tentatively identified by composition, $(U,Mo)Al_4$, (b) the Al-rich and (c) the U–Mo-rich side of the $(U,Mo)Al_4$ composition region.

The thickness of the interdiffusion zone developed in the diffusion couples annealed at 550°C for 24 hours have been measured by SEM. Shown in Table VI are the averaged thicknesses of the interdiffusion zones evaluated based on averaging of five linear measurements directly from the micrographs. Note that for the case of the U–10Mo vs. Al–6061 the average is based on three line measurements.

Table VII shows the averaged interdiffusion zone thickness based on measuring a typical area of the interdiffusion zone and then dividing that area by its width to obtain what, in order to differentiate the measurements, will be referred to as the integrated average thickness.

In Figure 13, the interdiffusion-layer thickness is plotted as a function of Mo concentrations in the U–Mo of the diffusion couples. Data from other experiments using Al and Al-5Si alloy were included for comparison. Generally speaking, the current data suggest that for the case of diffusion couples containing Al–6061 alloy, increased concentrations of Mo in the U–Mo alloy appear to reduce the growth rate of the interdiffusion zone.

Table VI. Thickness of interdiffusion zone measured from backscatter electron photo-micrographs by line measurements of the interdiffusion zones in couples annealed at 550°C for 24 hours.

Diffusion Couple	Line Averaged Thickness (μm)
U–7Mo vs. Al–6061	690±36
U–10Mo vs. Al–6061	432±30
U–12Mo vs. Al–6061	403±23

Table VII. Interdiffusion zone thickness measured from backscatter electron photomicrographs by area measurement of the diffusion couples annealed at 550°C for 24 hours.

Diffusion Couple	Integrated Average Thickness (μm)
U–7Mo vs. Al–6061	741
U–10Mo vs. Al–6061	400
U–12Mo vs. Al–6061	467

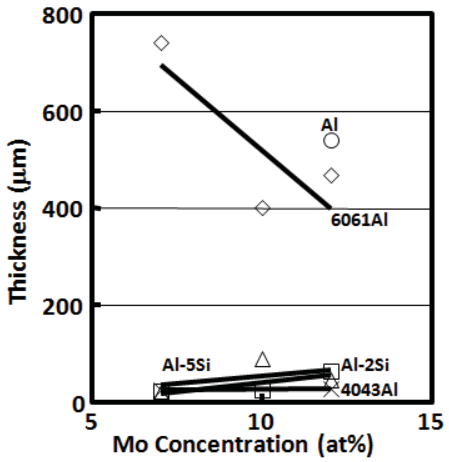

Figure 13. Effect of Mo concentration in the U–Mo alloy on the interdiffusion layer thickness of diffusion couples containing Al or Al alloys annealed at 550°C for 24 hours. (x: Al–4043; circle: pure Al; square: Al–2Si; triangle: Al–5Si; diamond: Al–6061).

3.1.2.1 Concentration Profiles, Interdiffusion Fluxes and Integrated Interdiffusion Coefficients

The experimental concentration profiles, after smoothing, of major components (namely U, Mo and Al) are presented in Figure 14(a) through Figure 16(a) for the U–7Mo vs. Al–6061, U–10Mo vs. Al–6061 and U–12Mo vs. Al–6061 couples, respectively. The interdiffusion fluxes were then determined directly from the concentration profiles, and are shown in Figure 14(b) through Figure 16(b). The integrated interdiffusion coefficients, $\tilde{D}^{int}_{i,\Delta x}$, of the major components were then determined from the interdiffusion flux profiles as reported in Table VIII. These coefficients represent cumulative interdiffusion fluxes across the intermetallic phase region.

The concentration profiles show that the diffusion couples developed interdiffusion zones with the average phase composition of $(U,Mo)Al_4$, with measurable concentrations of Mg and Si, similar to that previously observed in the diffusion couples annealed at 600°C for 24 hours. In these diffusion couples, Si diffused into the phase layer, and concentrated on the Al-rich side of the diffusion couple in the

intermetallic. The increase in Si concentration in this area resulted in a corresponding reduction of the Al concentration.

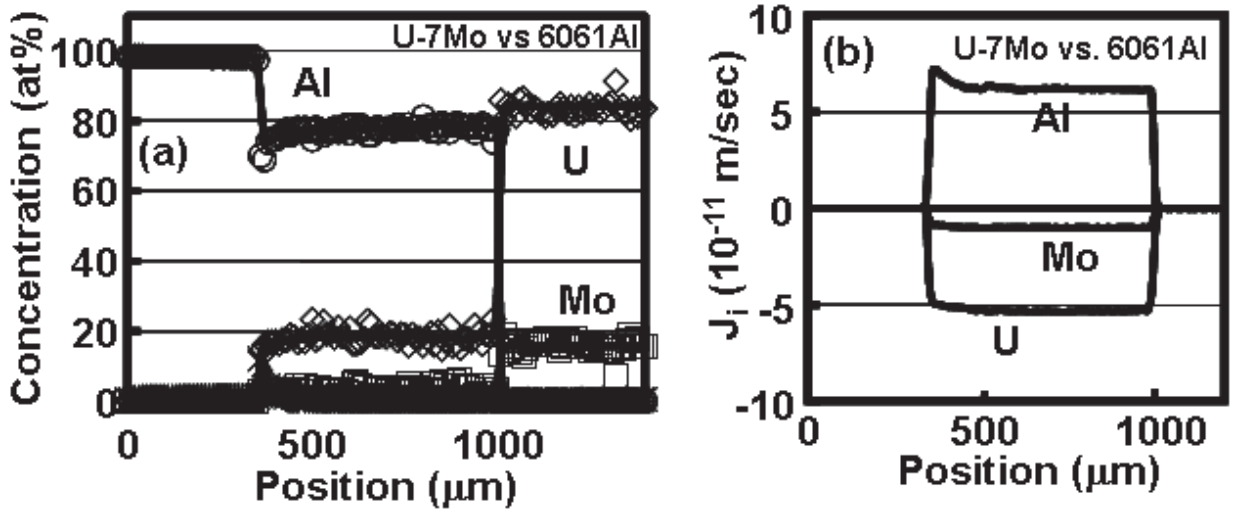

Figure 14. (a) Concentration profiles and (b) corresponding interdiffusion flux profiles from U–7Mo vs. Al–6061 diffusion couple annealed at 550°C for 24 hours.

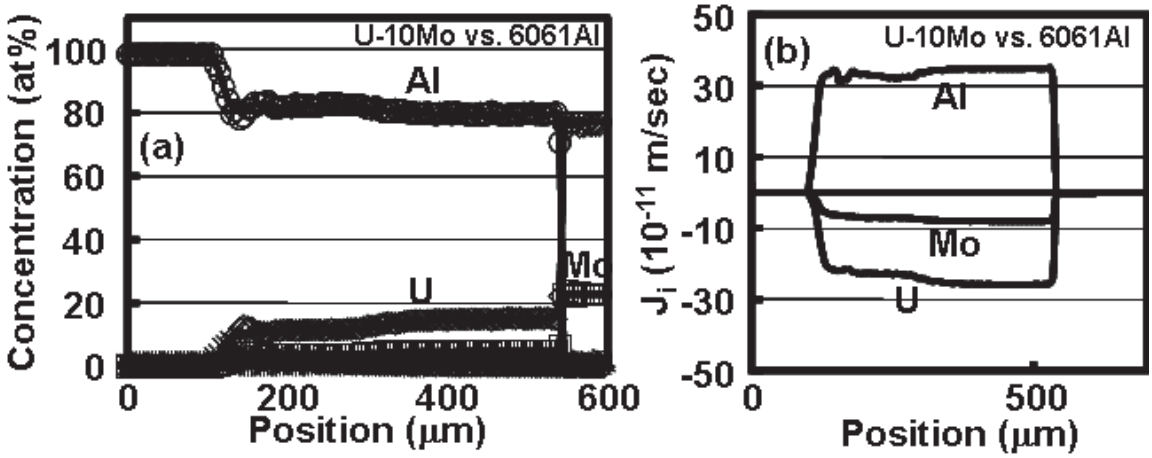

Figure 15. (a) Concentration profiles and (b) corresponding interdiffusion flux profiles from U–10Mo vs. Al–6061 diffusion couple annealed at 550°C for 24 hours.

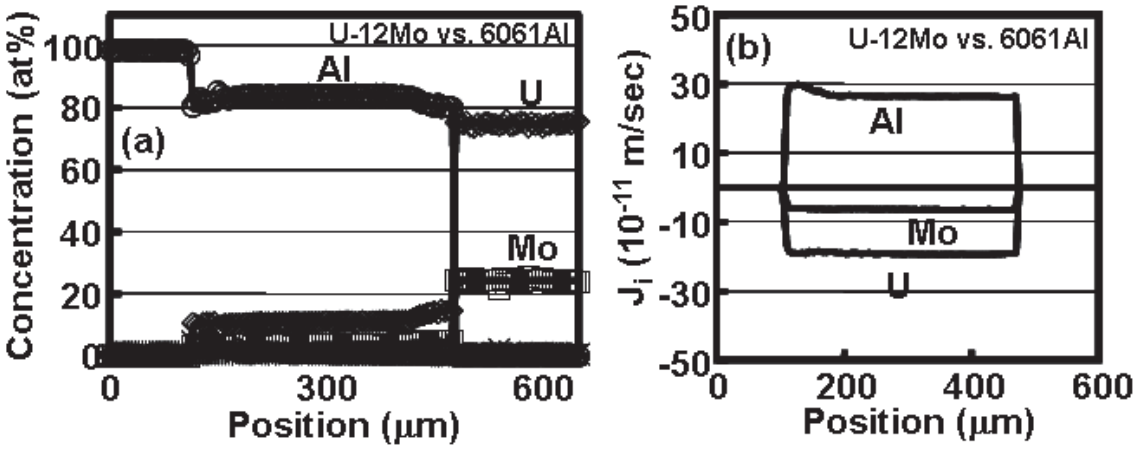

Figure 16. (a) Concentration profiles and (b) corresponding interdiffusion flux profiles from U–12Mo vs. Al–6061 diffusion couple annealed at 550°C for 24 hours.

Table VIII. Integrated interdiffusion coefficients $\tilde{D}_{i,\Delta x}^{int}$ of Al, Mo and U in the diffusion couples treated at 550°C for 24 hours. These integrated interdiffusion coefficients represent the cumulative interdiffusion fluxes across the intermetallic phase region.

Diffusion Couple (550°C for 24hr)	$\tilde{D}_{i,\Delta x}^{int}$ (10^{-16} m^2/sec)		
	Al	Mo	U
U–7Mo vs. Al–6061	4188.2	-662.5	-3535.8
U–10Mo vs. Al–6061	1473.3	-321.9	-1039.4
U–12Mo vs. Al–6061	1004.1	-109.1	-321.2

3.1.2.2 Energy Dispersive Spectroscopy Compositional Analysis of Phases Present in Interdiffusion Zone

The interdiffusion zones of the U–Mo vs. Al–6061 couples develop complex microstructures that appear to be the result of the different alloying additions present in the Al alloy. The maximum concentrations for the different alloying constituents, in atom percent, for Al–6061 are shown in Table IX. Standardless quantitative EDS analysis was performed on the interdiffusion zone of the U–7Mo vs. Al–6061 diffusion couple to supplement the collected EPMA data. As shown in Figure 17, the data were collected in a roughly linear manner from the Al-rich side to the U–7Mo (wt%) rich side of the diffusion couple. Care was taken so that data was collected on what appeared to be individual phases present in the interdiffusion zone. This, however, does not necessarily rule out interactions with other phases below the surface of the sample's cross-section. For the analysis, all the reported elements present in the Al–6061 and the U–7Mo were taken into account.

Table IX. Composition of the Al–6061 alloy showing the maximum concentrations of alloying additions.

Component	Amount (at%)
Al	96.92
Mg	1.34
Si	0.78
Fe	0.34
Cu	0.17
Zn	0.10
Ti	0.09
Mn	0.07
Cr	0.18
Others	Negligible

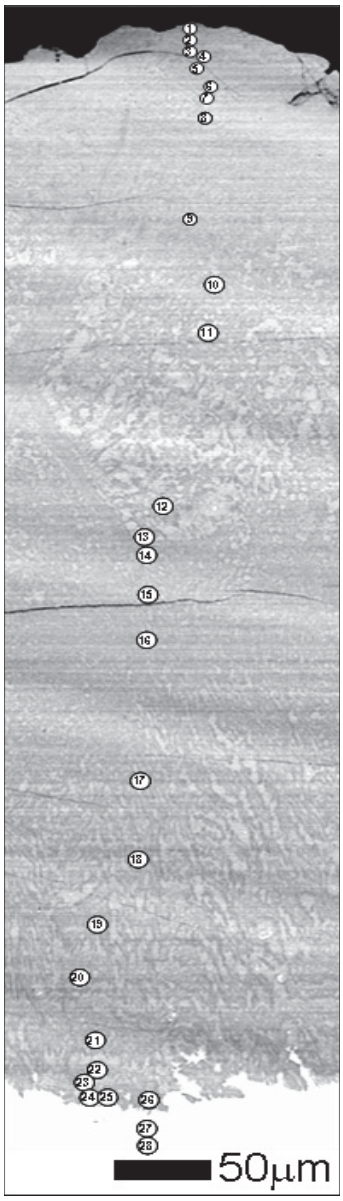

Figure 17. Backscatter electron micrograph of the interdiffusion zone for the U–7Mo vs. Al–6061 diffusion couple treated at 550°C for 24 hours, showing where the EDS data in Table X was collected.

Table X shows the composition of each point collected throughout the interdiffusion zone. The position of each point was then measured with respect to a random point chosen in the Al alloy, away from the interaction zone, and a preliminary concentration profile, shown in Figure 18, was then constructed based on the EDS data and the position where the data was collected linearly vertically down from the chosen point.

Table X. Composition of the individual data points collected by EDS on individual phases in the interdiffusion zone of the U–7Mo vs. Al–6061 diffusion couple treated at 550°C for 24 hours, and the averaged composition.

Data Point	Al	Mg	Si	Fe	Cu	Zn	Ti	Mn	Cr	U	Mo
Point 1	68.21	3.82	10.35	0.30	0.75	1.38	0.03	0.15	0.19	12.63	2.20
Point 2	67.58	3.96	9.28	0.55	0.87	1.60	0.27	0.36	0.24	12.57	2.71
Point 3	66.54	2.81	10.84	0.46	1.29	0.69	0.21	0.26	0.30	14.47	2.13
Point 4	64.08	4.20	10.78	0.19	1.38	1.61	0.13	0.23	0.00	14.49	2.91
Point 5	65.14	4.78	6.83	0.95	2.34	1.80	0.49	0.76	0.56	14.34	2.00
Point 6	70.73	4.29	3.98	0.61	1.91	1.60	0.42	0.40	0.40	13.32	2.34
Point 7	71.70	4.27	2.98	0.55	1.55	1.82	0.30	0.35	0.42	13.69	2.35
Point 8	72.74	3.56	2.07	0.49	1.28	1.57	0.00	0.29	0.43	15.01	2.54
Point 9	73.33	2.76	1.56	0.54	0.63	1.24	0.84	0.60	0.74	15.27	2.50
Point 10	67.78	4.35	2.21	1.23	0.84	1.89	0.69	0.82	1.00	15.31	3.87
Point 11	71.89	2.40	1.36	0.33	1.42	1.53	0.55	0.48	0.40	17.29	2.36
Point 12	73.48	3.22	0.97	0.19	0.53	1.63	0.32	0.28	0.18	16.08	3.13
Point 13	70.60	3.94	1.49	0.50	0.78	1.05	0.24	0.37	0.41	20.00	0.63
Point 14	74.18	3.79	1.30	0.56	0.99	1.48	0.00	0.15	0.32	14.98	2.26
Point 15	73.81	2.75	0.69	0.69	0.95	1.52	0.58	0.32	0.59	15.51	2.60
Point 16	75.10	2.80	0.73	0.58	0.21	1.29	0.45	0.25	0.42	14.95	3.22
Point 17	74.94	2.98	0.94	0.43	0.58	1.34	0.13	0.26	0.25	15.52	2.63
Point 18	73.84	2.63	1.02	0.56	0.76	1.62	0.22	0.39	0.46	15.86	2.65
Point 19	73.74	3.32	0.96	0.41	1.00	1.56	0.44	0.31	0.43	14.85	2.97
Point 20	71.25	2.99	1.29	0.39	0.69	1.15	0.66	0.46	0.33	20.02	0.78
Point 21	72.92	3.50	1.33	0.90	1.14	1.46	0.43	0.62	0.60	13.72	3.38
Point 22	74.30	3.09	1.43	0.26	0.70	1.63	0.36	0.41	0.18	14.66	2.97
Point 23	72.29	3.20	1.34	0.49	0.68	1.74	0.25	0.47	0.41	16.73	2.37
Point 24	73.38	3.15	1.05	0.78	1.13	1.62	0.20	0.30	0.73	14.70	2.97
Point 25	67.64	4.17	1.54	0.68	0.90	1.77	0.82	0.46	0.55	20.44	1.05
Point 26	72.32	3.69	1.29	0.71	0.42	1.69	0.71	0.56	0.53	14.32	3.76
Point 27	7.92	0.00	1.83	2.79	3.88	0.00	0.94	1.81	1.98	65.05	13.80
Point 28	5.23	4.85	4.48	2.19	3.19	3.11	1.25	2.08	0.89	61.78	10.97
Average Composition	71.29	3.48	3.06	0.55	0.99	1.51	0.37	0.40	0.43	15.41	2.51

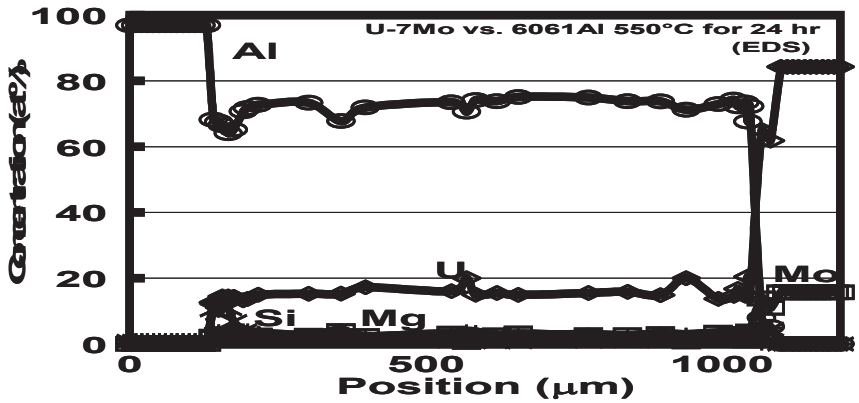

Figure 18. EDS generated concentration profile of the U–7Mo vs. Al–6061 diffusion couple treated at 550°C for 24 hours.

The deviations in the horizontal positioning of the EDS measurements were ignored with the assumption that the composition in the interdiffusion zone is constant through any horizontal section with respect to the figure. No measurements were made of the Al alloy. As a result, the data points presented in the concentration profile for the Al-alloy were plotted using the alloy composition shown in Table IX. Also in the U–7Mo alloy, only a few data points were collected. To complete the concentration profile, the U–7Mo composition was converted to atom percent and used in the chart. The collected EDS data is in close agreement with that collected by EPMA shown in Figure 14. The Al concentration in the EDS data shows a lower concentration roughly of 5 at.% as compared to the EPMA data. This may be the result of the additional components considered in the EDS analysis.

Based on the data shown in Table X, the interdiffusion zone of this diffusion couple shows higher concentrations of the trace elements, Mg, Si, Cu, Zn, Ti, Mn and Cr, than found in the Al–6061 alloy. Only the concentration of Fe remains similar to that found in the Al alloy, and it is found evenly distributed throughout the interdiffusion zone. It is worth noting that the concentrations of these trace elements are low and that the collected data may be within the error of the EDS collection equipment. For the cases of Mg, Si, Zn, Ti and Cu, however, qualitative analysis of the data, shown in Figure 19, indicates that there are small but distinctive excitation peaks for Mg, Si, Ti and Cu Kα and Zn Lα radiation. This confirms the fact that these elements are indeed present in the interdiffusion zone. Concentrations of Mg and Si are high in the Al-rich side of the interdiffusion zone between points 1 and 4. This area is marked by a multi-phase zone with fine precipitates. Between points 4 and 9, there is a microstructural change that is accompanied by a small increase in Cu concentration. Here, Mg and Si concentration remain higher than the average over the interdiffusion zone and decrease at point 9 where their values drop to those close to the average composition in the intermetallic phase. The higher concentration of Cu combined with high concentrations of Mg and Si may then explain the microstructure observed in this area. After point 9, another microstructural change is observed where a two-phase microstructure appears to have developed with relatively coarse precipitates. Between points 10 and 13, all alloying elements that are found in the Al-alloy appear to remain around the average composition found in the interdiffusion zone. This zone appears to be characterized by an increase in the U and Mo concentrations from that of the previous points, and above the average concentration of the interdiffusion zone. Between points 14 and 26, another microstructural change appears to take place. Here a two- or three-phase microstructure

exists, where the precipitates grow in size as one moves towards the (U,Mo)-rich area. Throughout this area, the trace elements from the Al alloy and the U–7Mo alloy remain close to their average concentration in the interdiffusion zone. Note that the value of the Si average concentration is heavily affected by the strong increase in concentration in the Al-rich area of the interdiffusion zone and that the average concentration below this zone is similar to that found in this between points 10 and 26. In U–7Mo alloy at points 27 and 28, high concentration of Mg, Si, Fe, Cu, Zn, Ti and Mn are observed at levels higher than the average in the intermetallic phase and in the Al-alloy. Further data points were not collected.

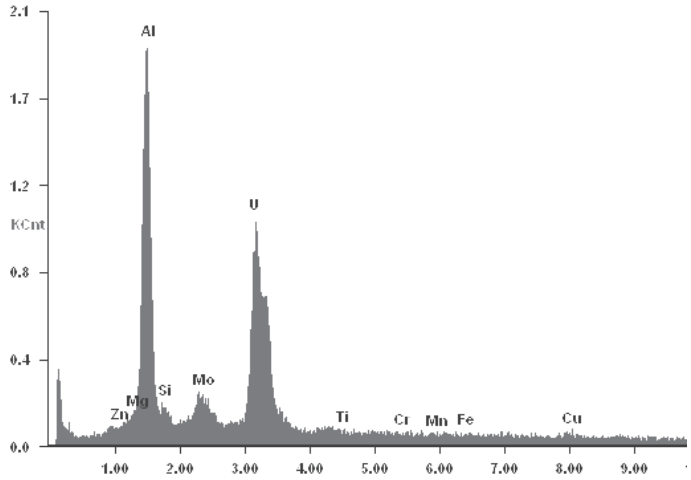

Figure 19. Typical EDS pattern of the collected data for the U–7Mo vs. Al–6061 diffusion couple treated at 550°C for 24 hours.

3.1.3 Diffusion Couples Annealed at 500°C for 132 Hours

Diffusion couples of U–7Mo, U–10Mo and U–12Mo vs. Al–6061 have been assembled and annealed at 500°C for 132 hours. Figure 20 through Figure 22 show backscatter electron micrographs of the diffusion couples with detailed micrographs showing both the interfaces between the Al alloy and the interdiffusion zone and the interface between the U–Mo alloy and interdiffusion zone for those diffusion couples treated at 500°C for 132 hours.

In the U–7Mo vs. Al–6061 and U–10Mo vs. Al–6061 couples, the U–Mo alloy may have undergone decomposition from the γ–U to the (α-U + δ-U_2Mo) phases. In these couples, the interface between the U–Mo alloy and intermetallic phase shows regions of complex microstructure that may indicate that the phase transformation in U–Mo alloy has taken place.

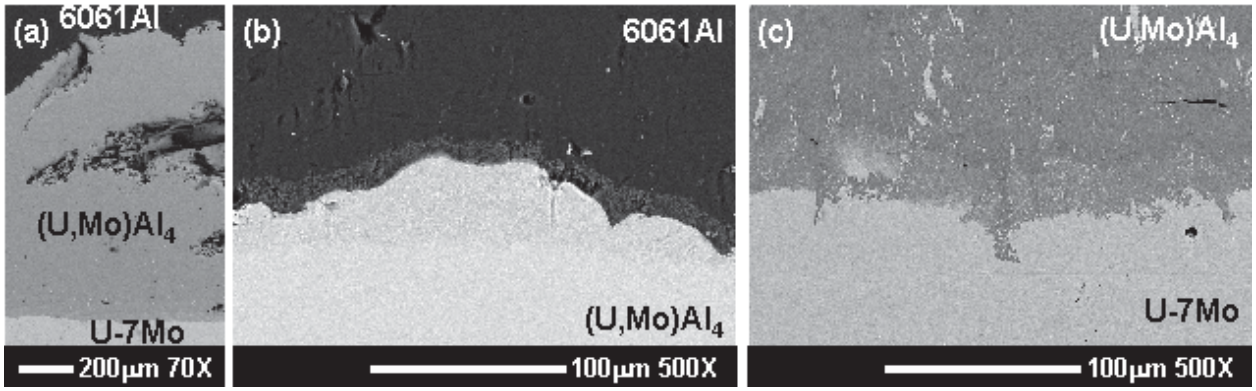

Figure 20. Backscatter electron micrographs of the U–7Mo vs. Al–6061 diffusion couple annealed at 500°C for 132 hours showing: (a) the entire interdiffusion zone containing, tentatively identified by composition, $(U,Mo)Al_4$, (b) the Al-rich and (c) the U–Mo-rich side of the $(U,Mo)Al_4$ composition region.

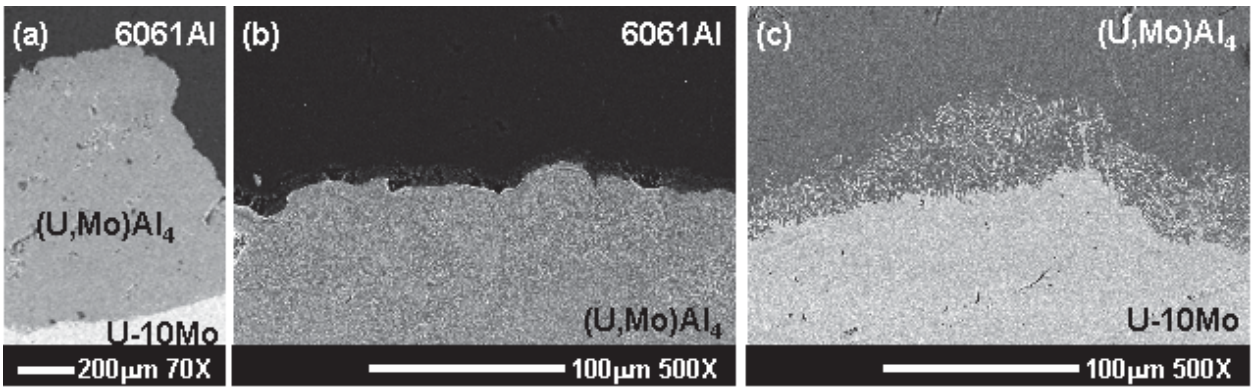

Figure 21 Backscatter electron micrographs of the U–10Mo vs. Al–6061 diffusion couple annealed at 500°C for 132 hours: showing (a) the entire interdiffusion zone containing, tentatively identified by composition, $(U,Mo)Al_4$, (b) the Al-rich and (c) the U–Mo-rich side of the $(U,Mo)Al_4$ composition region.

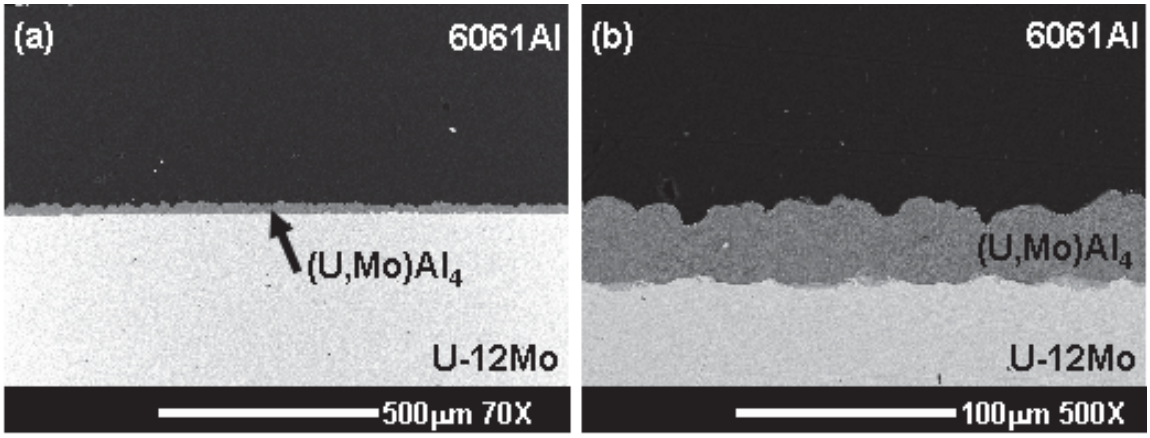

Figure 22. Backscatter electron micrographs of the U–12Mo vs. Al–6061 diffusion couple annealed at 500°C for 132 hours: showing (a) the entire interdiffusion zone containing, tentatively identified by composition, $(U,Mo)Al_4$, (b) detailed micrograph of the interdiffusion zone.

The thickness of interdiffusion zone developed in diffusion couples annealed at 500°C for 132 hours have been measured by SEM. Table XI shows the averaged interdiffusion zone thickness based on measuring a typical area of the interdiffusion zone by image processing and then dividing that area by its width to obtain the integrated average thickness. Measurements for the diffusion couples did not include regions of limited interaction. As in the diffusion couples tested at higher temperatures, the diffusion couples containing the Al–6061 alloy developed the interdiffusion zones with thick interaction zones between the alloys.

Table XI. Interdiffusion zone thickness measured from backscatter electron photomicrographs by area measurement of the diffusion couples treated at 500°C for 132 hours.

Diffusion Couple	Integrated Average Thickness (μm)
U–7Mo vs. Al–6061	1127
U–10Mo vs. Al–6061	575
U–12Mo vs. Al–6061	28

3.2 Comparison of Microstructural Features for Diffusion Couples Prepared with and without Nitric Acid Treatment of the Al–6061

As described earlier, a sample preparation experiment was carried out to determine the optimal parameters for diffusion couple assembly. In order to make a comparative study, the Al–6061 and uranium alloys were polished with diamond paste to 1μm before the acid treatment was performed. The Al–6061 and uranium alloys were then treated with concentrated nitric acid to remove the oxide layers that develop on the alloy surfaces due to exposure with air. The alloys, after treatment, shown in Figure 23, exhibited different behavior. The Al–6061 alloy surfaces appeared visually clean. It is expected that the Al_2O_3 layer was successfully dissolved. The uranium alloy, on the other hand, developed a layer on the surface that appeared brownish and dull, indicating that a reaction layer developed after treatment. This section describes the results for diffusion couples annealed using samples prepared using two different processes.

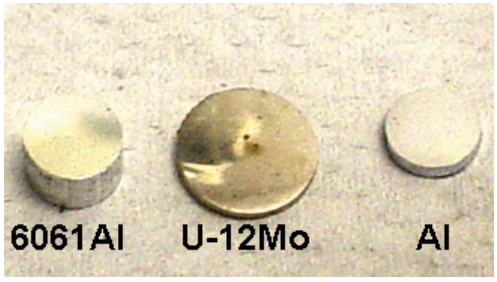

Figure 23. Diffusion couple alloys after nitric acid treatment of the surfaces.

3.2.1 Diffusion Couples Between U–12Mo and Al–6061 Annealed at 600°C for 24 Hours

Treating the alloy surfaces with nitric acid was expected to dissolve the oxide layers that develop on the Al and U–Mo alloys. This was expected to improve bonding of the alloys during diffusion anneal, leading to larger interaction zones between the alloys. To obtain an understanding of the effect of cleaning the surfaces with nitric acid, comparisons were made between U–12Mo vs. Al–6061 couples

assembled and annealed at 600°C for 24 hours, comprised of Al–6061 alloy disks that were treated or un-treated with nitric acid.

Initially, the Al–6061 and U–Mo alloys were polished to 1 μm using diamond paste in an Ar atmosphere. After polishing, the alloys would have been in the same condition that was previously prerequisite to assembling diffusion couples. After polishing, the Al–6061 was treated with concentrated nitric acid. Based on the results mentioned above that indicate that the U–Mo alloy reacts negatively to the acid treatment, the U–Mo alloy was re-polished with 1μm diamond paste and was not treated with acid. The U–Mo was used in the as-polished condition to assemble the diffusion couple.

After diffusion annealing, the diffusion couple was cross-sectioned and polished using the standard procedures. A composite backscatter electron micrograph of the developed interaction zone between the alloys is shown in Figure 24. Excellent bonding was achieved between the alloys. The developed interface was continuous and evenly distributed throughout the interaction zone except at the ends of the zone, where edge effects of the terminal alloys may have played a factor in the interdiffusion behavior.

Shown in Figure 25 is a composite backscatter electron micrograph of the same diffusion couple shown in Figure 3. This diffusion couple was assembled using the standard assembly procedure where the alloys are only polished in an Ar atmosphere before assembly of the couple. This couple was treated at the same time and temperature as that of the couple that was treated with nitric acid. Comparison of the diffusion couples shows that the couple where nitric acid was used developed a significantly smaller, but more uniform, interaction zone. The acid treated interaction zone is 488μm thick while the non-treated diffusion couple developed a zone 925μm thick. This appeared to contradict the expected results where the treated couple should have developed a larger interaction zone due to better removal of the oxide layers on the alloys surfaces.

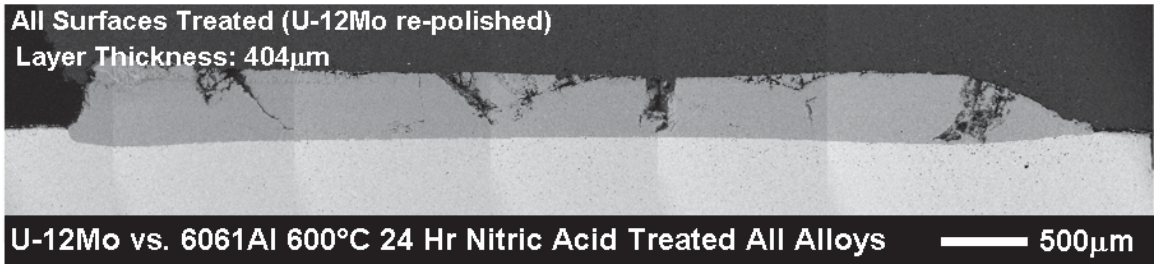

Figure 24. U–12Mo vs. Al -6061 annealed at 600°C for 24 hours with the Al–6061 treated with nitric acid before assembly.

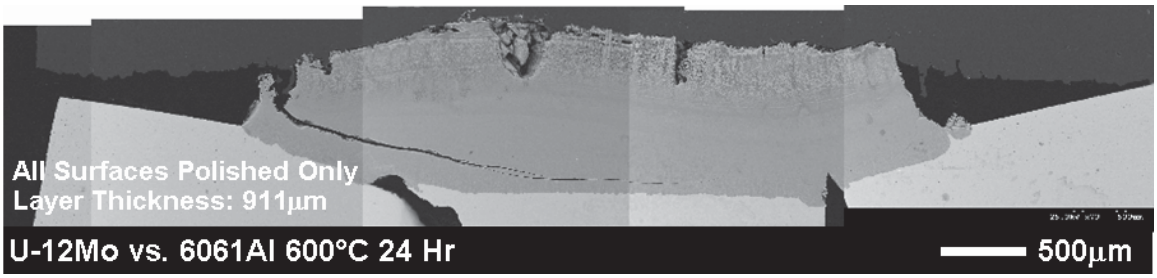

Figure 25. U–12Mo vs. Al–6061 annealed at 600°C for 24 hours with the Al–6061 only polished before assembly.

Because of the results described above, two new sets of U–12Mo vs. Al–6061 diffusion couples were assembled and annealed. One diffusion couple was prepared by using only polishing of all the alloys (i.e.,

without nitric acid bath). Another couple was prepared by treating the Al alloy with nitric acid. Based on the earlier evaluation of the effects of nitric-acid treatment on the surface of different alloy samples, the U–12Mo alloy was only polished and cleaned without exposure to nitric acid. Furthermore, all the diffusion couples were encased in the same quartz capsule to provide identical annealing conditions. The couples were then annealed at the same time and temperature as were the previous couples.

For the case of the diffusion couples only polished before annealing (Figure 25 and Figure 26), both alloys developed similar microstructures. In both cases, diffusion took place in a significant area of the couples, but the area did not cover the whole of the cross-sections where the alloys had initially been in contact. The initial diffusion couple developed a 911 μm thick layer while that of the second couple was 1072 μm. A 17.7% difference in layer thickness was observed. The nature of this discrepancy is not well understood, but fracturing and healing of the interaction layer could influence growth of the interdiffusion zone.

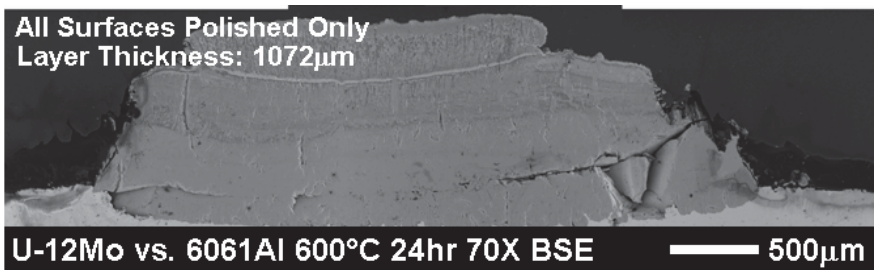

Figure 26. U–12Mo vs. Al–6061 annealed at 600°C for 24 hours with the Al–6061 polished only before assembly.

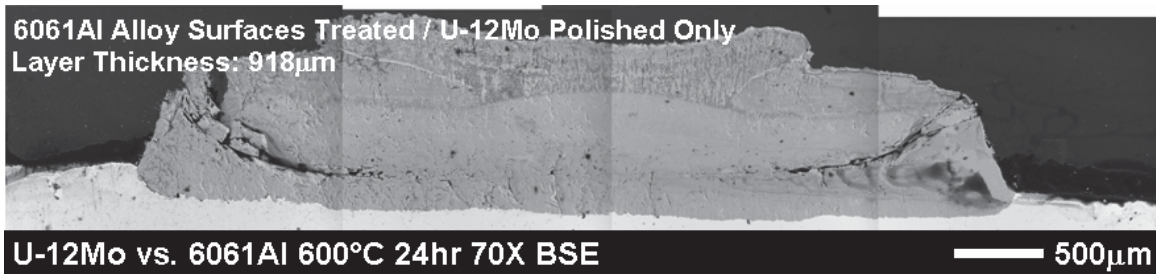

Figure 27. U–12Mo vs. Al–6061 annealed at 600°C for 24 hours where the Al–6061 was treated with nitric acid before assembly and the U–12Mo alloy was only polished.

Based on the results of this study, where more uniform diffusion zones were produced using a nitric acid treatment on the Al–6061 (see Figure 24 and Figure 27), the assembly procedure for all future diffusion couples, including those from other diffusion studies that employed pure Al and Al-Si alloys, was modified. During diffusion couple assembly, all Al–6061 samples from this point on in this document were immersed in concentrated nitric acid for several minutes to dissolve the oxides on the alloy's surfaces. The U–Mo alloys were polished immediately before the couples were assembled to mechanically remove the oxides on the alloy surfaces.

3.3 MICROSTRUCTURAL FEATURES FOR COUPLES WITH NITRIC ACID-TREATED Al–6061

3.3.1 Diffusion Couples Annealed at 600°C for 24 Hours

Diffusion couples of U–7Mo, U–10Mo, and U–12Mo vs. Al–6061 were annealed at 600°C for 24 hours in order to obtain large interdiffusion zones and to avoid decomposition of the γ-U phase. Figure

28 shows backscatter electron micrographs of the developed interaction regions from each diffusion couple. The gray contrast regions in the backscatter electron micrographs that define the interaction zones lie between the Al–6061 (top) and the U–Mo (bottom) alloys. These micrographs show that each diffusion couple achieved consistent bonding throughout the width of the diffusion couples. The interaction regions of the couples containing U–7Mo, U–10Mo, and U–12Mo developed thicknesses of 700 μm, 659 μm, and 694 μm, respectively. Based on the assumption of the parabolic growth rate, the growth constants for the diffusion couples containing U–7Mo, U–10Mo, and U–12Mo were calculated to be 2.38, 2.24, and 2.36 μm/sec^{½}, respectively. Comparison with results for the earlier diffusion couples using polished-only samples (section 3.1), it can be seen that the interaction zones are similar in thickness with the exception of the U–10Mo vs. 6061Al diffusion couple, where the new couple is only 57% the thickness of the initial one, but developed more consistent interdiffusion zones.

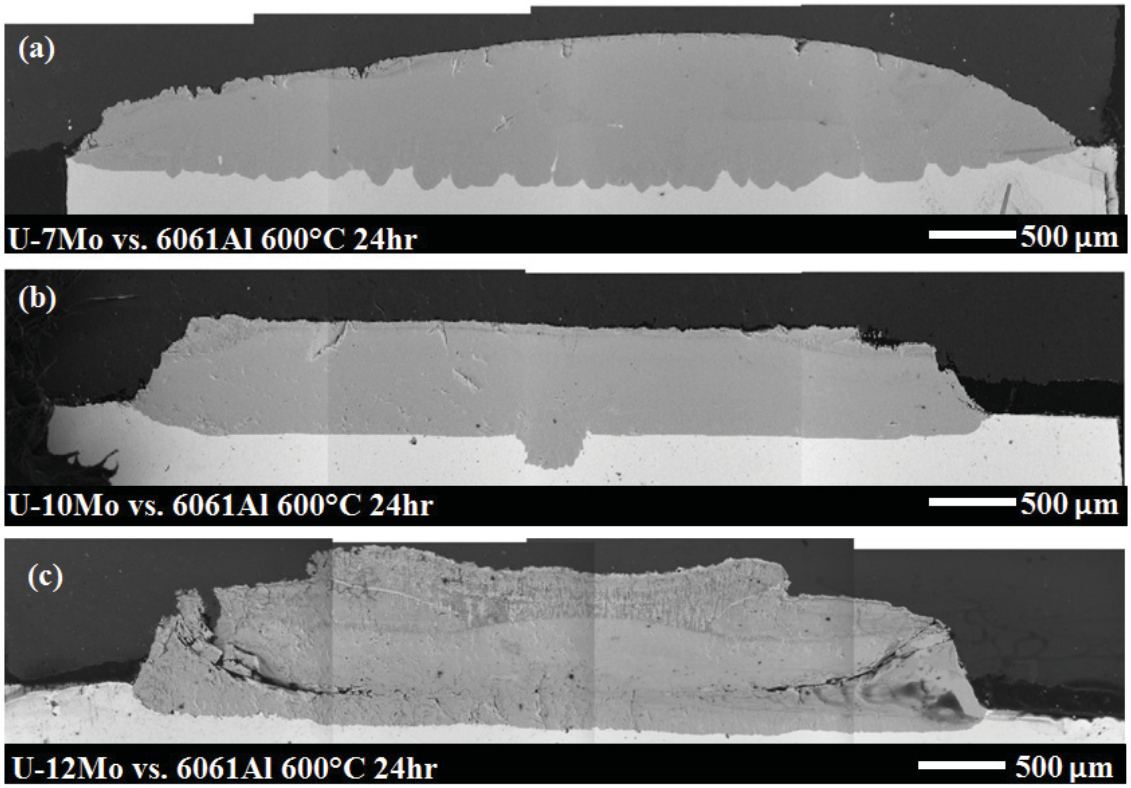

Figure 28. Backscatter electron micrographs of the (a) U–7Mo vs. Al–6061, (b) U–10Mo vs. Al–6061, and (c) U–12Mo vs. Al–6061 diffusion couples annealed at 600°C for 24 hours.

Close examination of the interaction regions show that they developed complex fine-grained multiphase microstructures. Figure 29, Figure 30, and Figure 31 show detailed micrographs of the interaction regions in the U–7Mo, U–10Mo, and U–12Mo vs. Al–6061 diffusion couples, respectively. The micrographs show, in progressive order, the changes in microstructures in the interaction regions from the Al–6061 side to the U–Mo side. Based on phase contrast, the interaction regions developed fine-grained multiphase microstructures encompassing several phases with significant compositional differences.

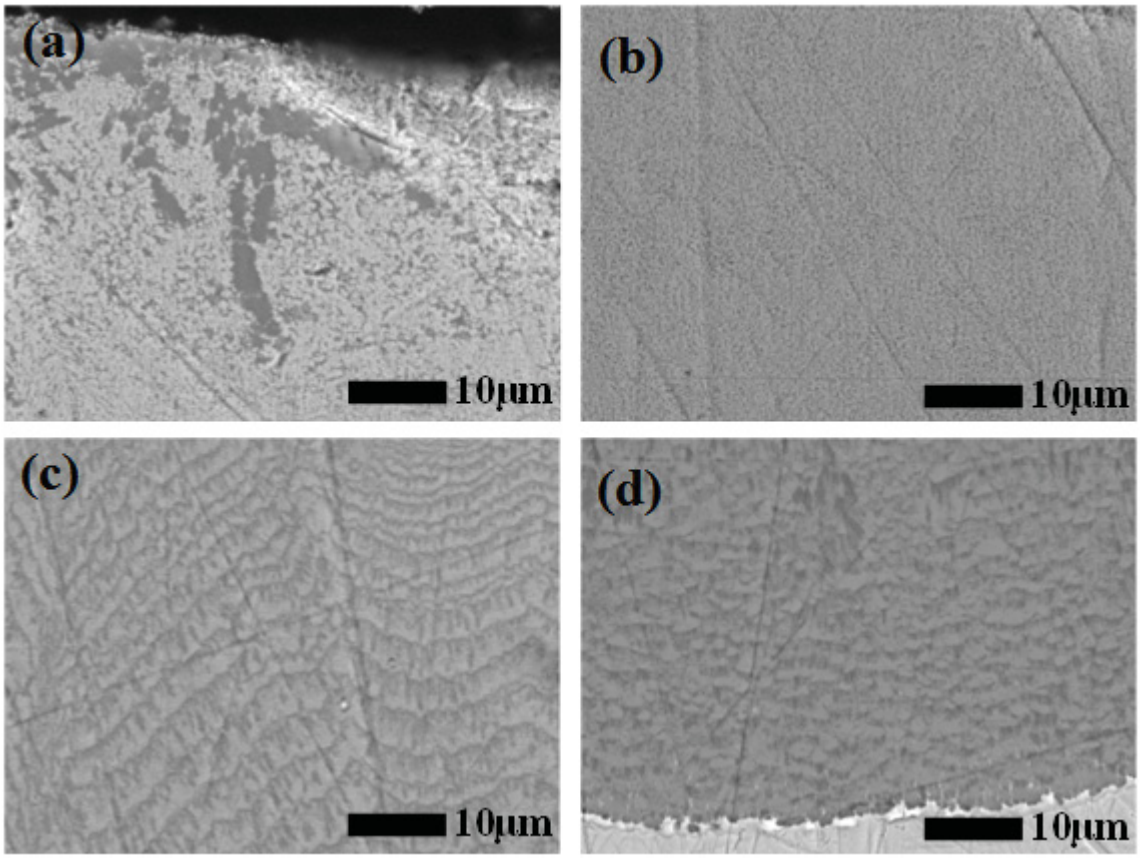

Figure 29. Detailed backscatter electron micrographs from the interaction region in the U–7Mo vs. Al–6061 diffusion couple annealed at 600°C for 24 hours. Changes in microstructures (a through d) are documented from the Al–6061 side to the U–7Mo side of the interaction region.

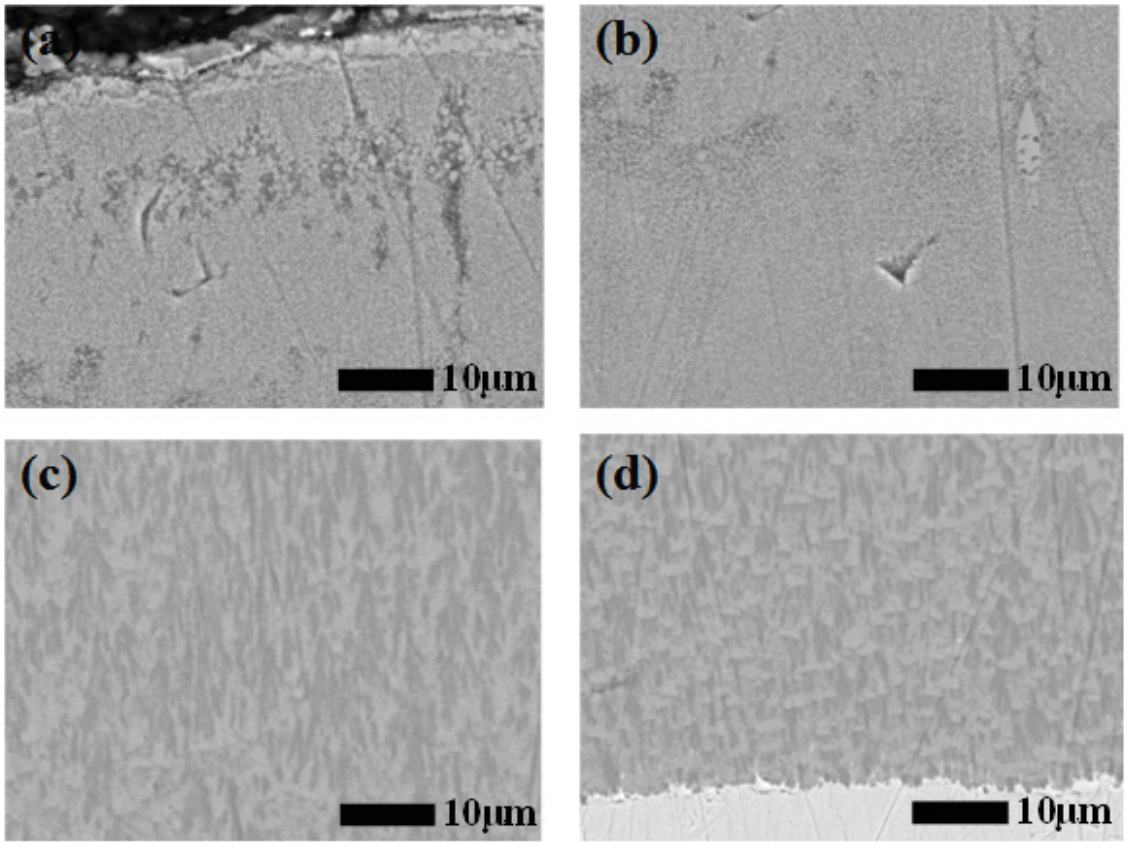

Figure 30. Detailed backscatter electron micrographs from the interaction region in the U–10Mo vs. Al–6061 diffusion couple annealed at 600°C for 24 hours. Changes in microstructures (a through d) are documented from the Al–6061 side to the U–10Mo side of the interaction region.

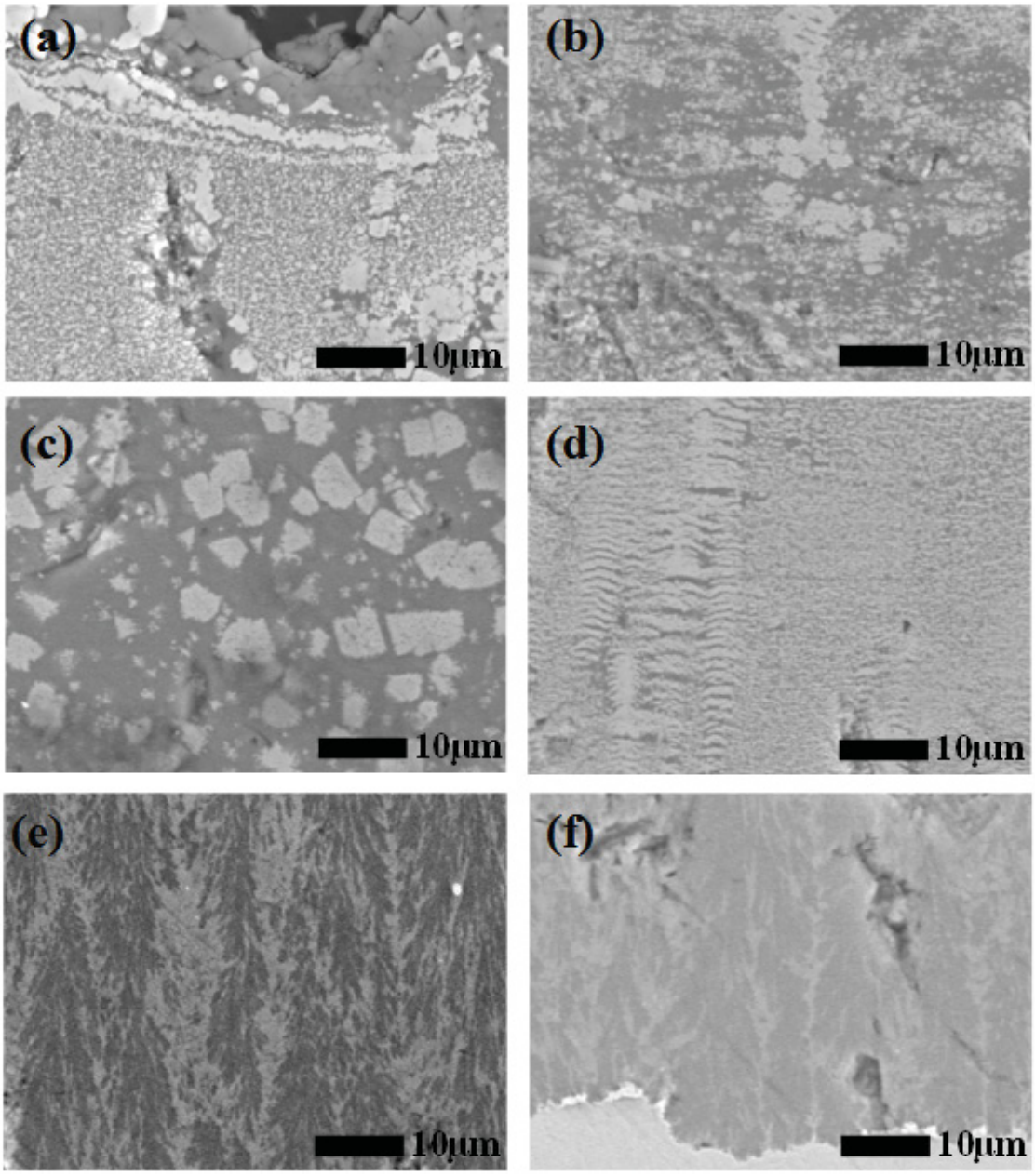

Figure 31. Detailed backscatter electron micrographs from the interaction region in the U–12Mo vs. Al–6061 diffusion couple annealed at 600°C for 24 hours. Changes in microstructures (a through f) are documented from the Al–6061 side to the U–12Mo side of the interaction region.

The U–12Mo vs. Al–6061 diffusion couple was analyzed in detail by EDS to determine the compositions of the apparently distinctive phases on the backscatter electron micrographs. This couple was chosen for analysis because the precipitates were relatively large, considering the interaction volume of the electron beam in the SEM. The measured compositions are summarized in Table XII. Because of the experimental uncertainty in the EDS analysis, measured concentrations lower than 1% are not reported. Figure 32 shows the general region where EDS data was collected. The regions marked by squares show specifically where data was collected. Figure 33 shows the detailed locations where each EDS measurement was carried out. Careful consideration was given to interpret the data correlating the

phase contrast in the backscatter electron micrographs and the measured compositions. Based on extensive analysis, a large number of phases were determined to be present in the interaction region. Up to 9 different groups of compositions were observed as reported in Table XII. Each composition is tentatively identified as a distinct phase and is represented by a Greek letter symbol. Given the interaction volume of the electron beam, some of the reported values may represent the average compositions of neighboring phases, whose grain size was too small to be measured accurately. This indicates the possibility that a larger number of phases exist in the interaction region.

Table XII. Compositions of the observed phases in the U–12Mo vs. Al–6061 diffusion couple measured by EDS.

Element	Phase α	Phase β	Phase γ	Phase δ	Phase ε	Phase η	Phase λ	Phase θ	Phase κ
Zn	2.8 ± 1.0	1.1 ± 0.4	0.9 ± 0.3	1.1 ± 0.3	-	1.6 ± 0.6	-	-	1.4 ± 0.4
Mg	4.3 ± 0.9	4.5 ± 0.4	4.0 ± 0.2	6.0 ± 0.2	-	-	-	-	-
Al	52.1 ± 1.7	81.3 ± 1.3	83.8 ± 0.7	71.9 ± 0.6	98.0 ± 0.3	59.7 ± 1.9	74.5 ± 0.8	83.0 ± 0.9	62.8 ± 2.5
Si	16.9 ± 1.0	-	-	1.3 ± 0.4	-	10.3 ± 1.6	-	-	7.4 ± 1.1
Mo	-	5.1 ± 0.2	-	-	-	-	6.6 ± 0.2	7.6 ± 0.6	1.0 ± 0.3
U	18.0 ± 1.2	4.1 ± 0.4	3.9 ± 0.2	5.0 ± 0.3	-	25.1 ± 0.6	15.4 ± 0.3	5.4 ± 0.3	23.0 ± 1.7
Ti	-	-	-	-	-	-	-	-	-
Cr	-	-	3.6 ± 0.4	-	-	-	-	-	-
Mn	-	-	-	-	-	-	-	-	-
Fe	1.1 ± 0.4	1.0 ± 0.2	-	13.6 ± 0.7	-	-	-	-	1.1 ± 0.2
Cu	1.9 ± 0.7	-	-	-	-	-	-	1.2 ± 0.2	1.1 ± 0.2

In Table XII, phase α represents the bright contrast phase observed near the interaction region interface with the Al–6061. This phase was depleted of Mo, contained high concentrations of Si, and had measurable concentrations of Cu, Fe, Mg, and Zn. Phase β represents the mid-gray contrast phase in the interaction region near the interface with the Al–6061. This phase is marked by low U and Mo concentrations and measurable concentrations of Fe, Mg, and Zn. Phase γ contained high Al concentration with some Cr and U. Phase δ is differentiated by a high concentration of Fe and Mg. Phase ε shows the Al–6061 composition near the interface with the interaction region where only small concentrations of the alloying additions of the Al–6061 were observed. Phase η developed high concentrations of Si, some Zn, and lacked measurable concentrations of the other alloying additions of the Al–6061. This phase region can be described to have an average composition near $U(Al,Si,Zn)_3$. Phase θ contained mainly U, Mo, and Al, with only a low concentration of Cu. Phase κ contained Si and trace amounts of Fe, Cu, and Zn. This composition may be grouped into an approximate average concentration

of $(U,Mo)(Al,Si)_3$. This average composition, with and without Mo, has been reported in other studies [92]. Phase λ lacked any of the minor alloying additions of the Al–6061. The average composition of the interdiffusion zone in this region can be summarized as $(U,Mo)Al_3$.

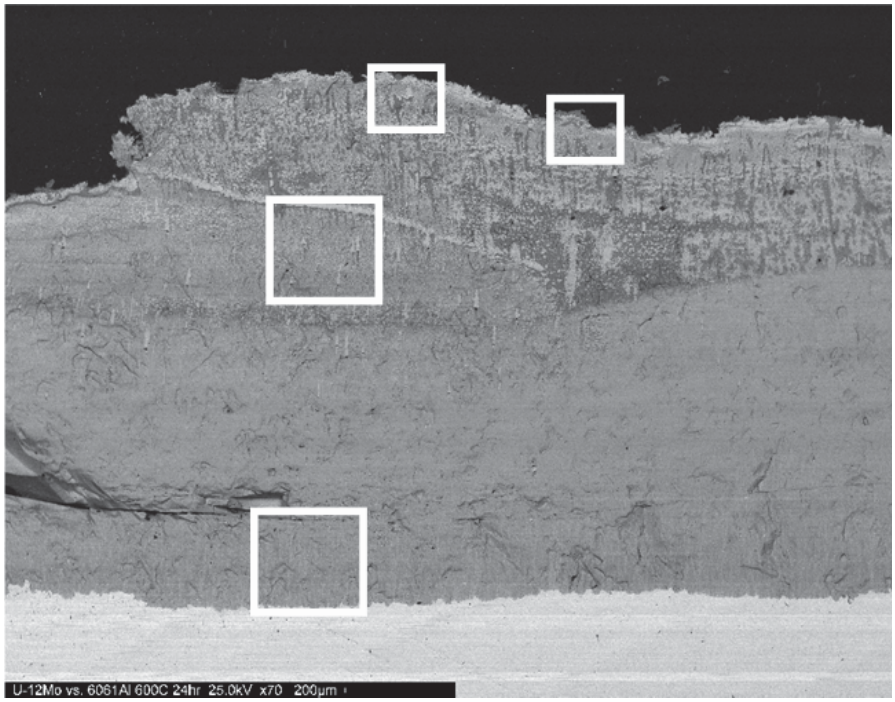

Figure 32. Backscatter electron micrograph of the U–12Mo vs. Al–6061 diffusion couple annealed at 600°C for 24 hours. The white rectangles mark the selected regions for EDS analysis.

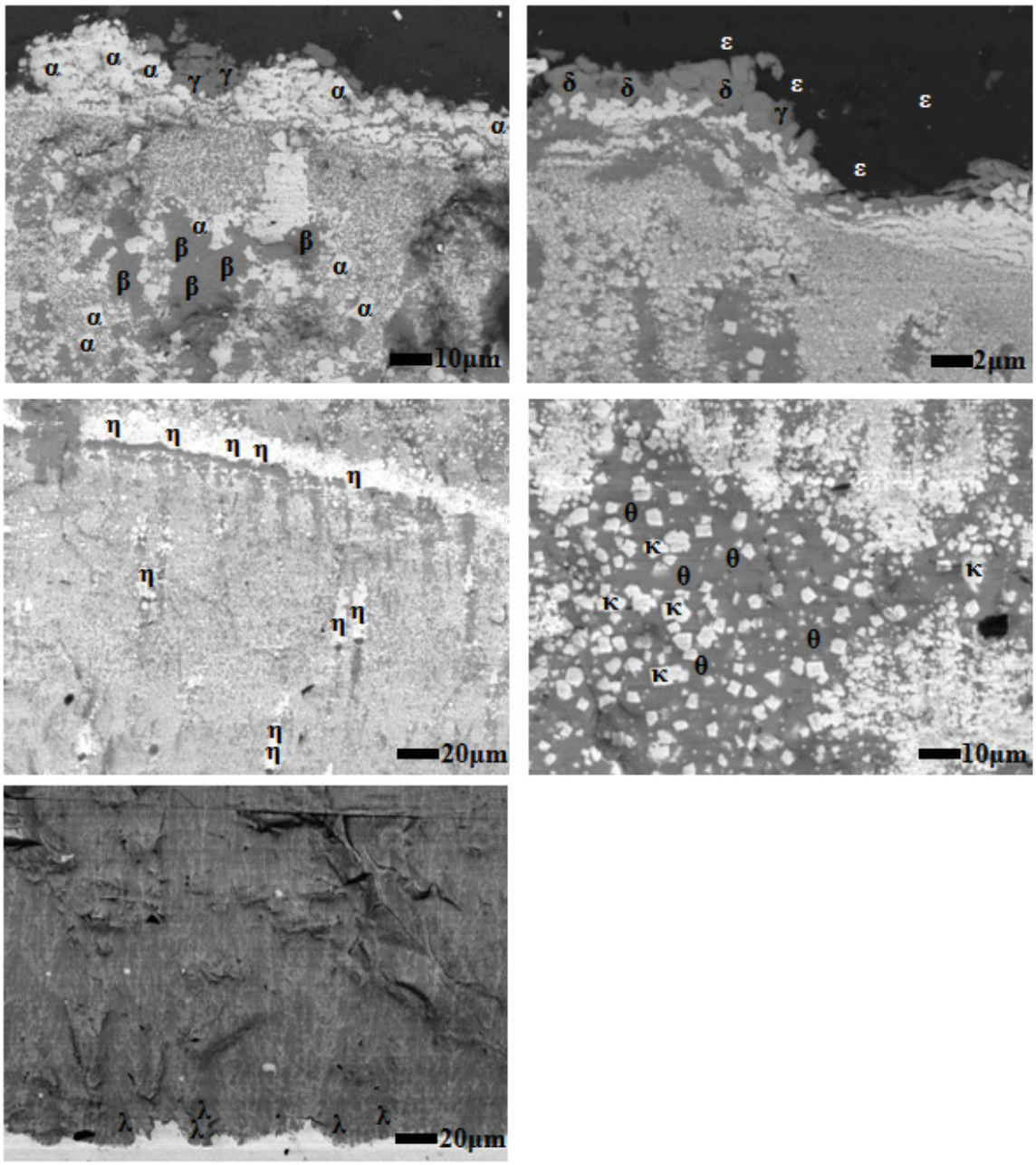

Figure 33. Backscatter electron micrographs of the U–12Mo vs. Al–6061 diffusion couple showing the locations where the EDS data in Table XII were collected.

Concentration profiles were determined by WDS for the U–7Mo vs. Al–6061 diffusion couple. The alloying additions typically found in the Al–6061 were measured (i.e., Al, Cr, Cu, Fe, Mg, Mn, Mo, Si, Ti, U, and Zn). Figure 34(a) shows the measured concentration profiles for major components, while Figure 34(b) details the elements found at low concentrations. Elements that did not show measurable concentration profiles in the interaction region are not reported. The concentration profiles show that Cu, Fe, Mg, and Si penetrated approximately 400μm into the interaction region. The region near the Al–6061 corresponds to the area shown in Figure 29(a), where several phases appear to have developed that contained Cu, Fe, Mg, and Si.

Comparison of Figure 29 with Figure 31(a) and Figure 33 shows that the region developed similar phase constituents, enriched with the alloying additions of the Al–6061, as those observed in the U–12Mo vs. Al–6061 diffusion couple.

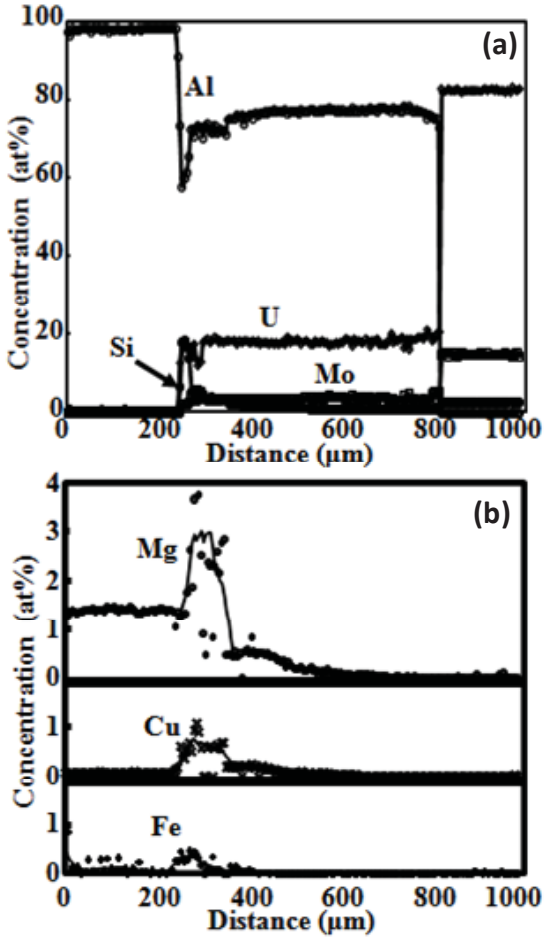

Figure 34. Concentration profiles of the U–7Mo vs. Al–6061 diffusion couple annealed at 600°C for 24 hours, showing (a) elements in high concentrations and (b) elements in low concentrations.

3.3.2 Diffusion Couples Annealed at 550°C for 1, 5, and 20 Hours

Diffusion couples of U–7Mo U–10Mo and U–12Mo vs. Al–6061 were assembled and annealed at 550°C for 1, 5, and 20 hours. Backscatter electron micrographs have been collected, the average thicknesses of the interdiffusion zones have been measured, and the Si distribution in some diffusion couples was observed through x-ray mapping. Table XIII summarizes the diffusion couples annealed at 550°C for 1, 5 and 20 hours. With the exception of a few couples (marked as N/A), the developed interdiffusion zones in the diffusion couples were consistent through the cross-sections of the couples. Figure 35 through Figure 41 show backscatter electron micrographs of the diffusion couples included in Table XIII.

Table XIII. Measured thickness of the IDZ in the diffusion couples annealed at 550°C for 1, 5 and 20 hours.

Diffusion Couple	550°C for 1 hour	550°C for 5 hours	550°C for 20 hours
	Thickness (μm)		
U–7Mo vs. Al–6061	9.6 ± 1.3	9.3 ± 1.1	141.5 ± 85.2
U–10Mo vs. Al–6061	*N/A*	8.8 ± 8.6	348.3 ± 114.2
U–12Mo vs. Al–6061	*N/A*	2.0 ± 0.4	312.4 ± 7.1

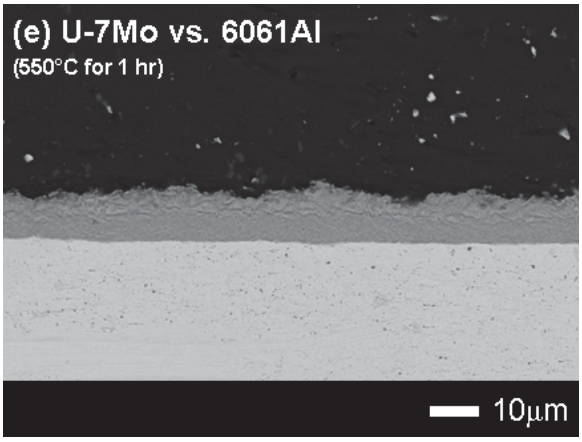

Figure 35. Backscatter electron micrographs of the interdiffusion zone for a U–7Mo vs. Al–6061 diffusion couple annealed at 550°C for 1 hour.

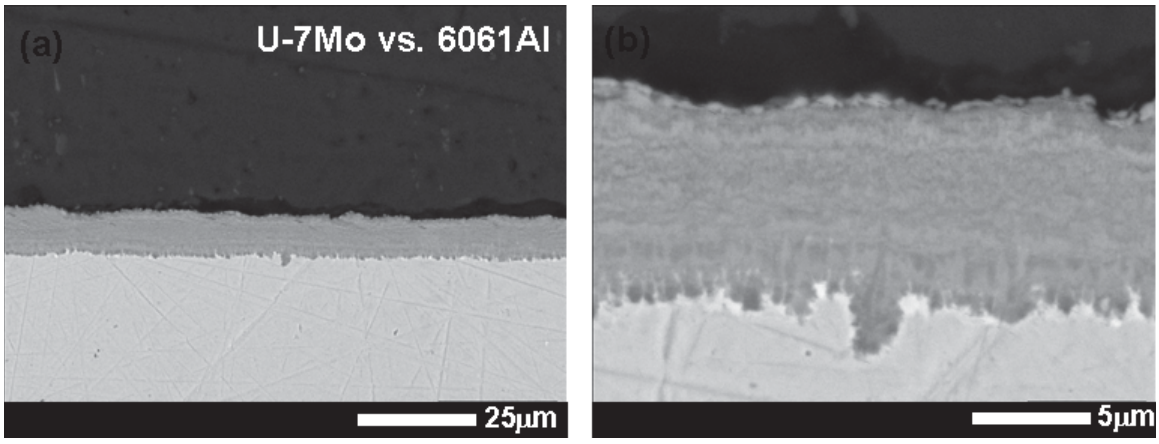

Figure 36. Backscatter electron micrographs of the interdiffusion zone for a U–7Mo vs. Al–6061 diffusion couple annealed at 550°C for 5 hours.

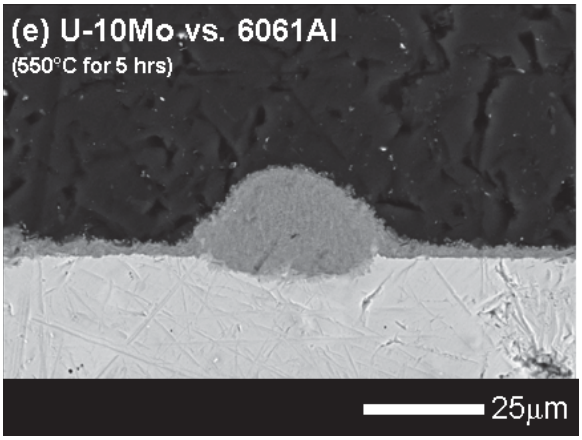

Figure 37. Backscatter electron micrograph of the interdiffusion zone for a U–10Mo vs. Al–6061 diffusion couple annealed at 550°C for 5 hours.

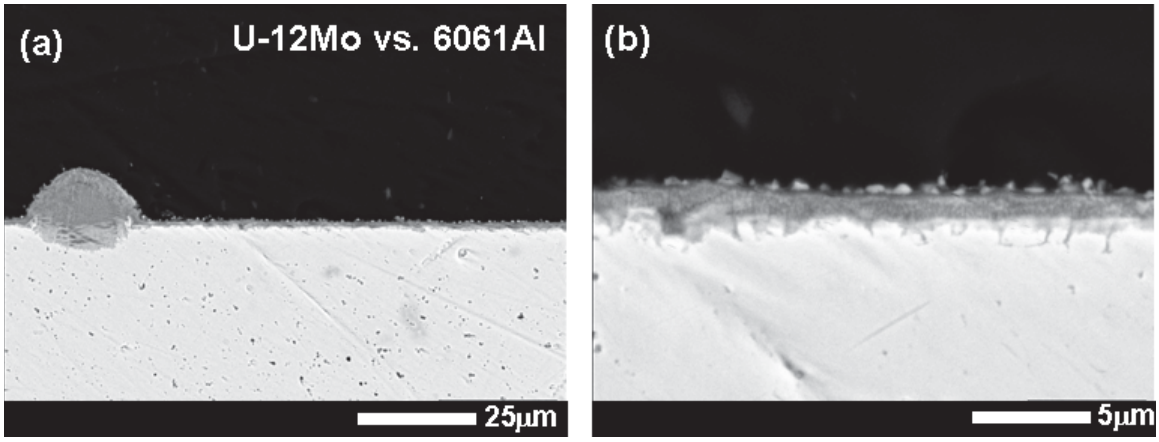

Figure 38. Backscatter electron micrographs of the interdiffusion zone for a U–12Mo vs. Al–6061 diffusion couple annealed at 550°C for 5 hours. (a) shows a localized region with higher thickness, and (b) shows a higher magnification image of the more uniformly-thick interdiffusion zone.

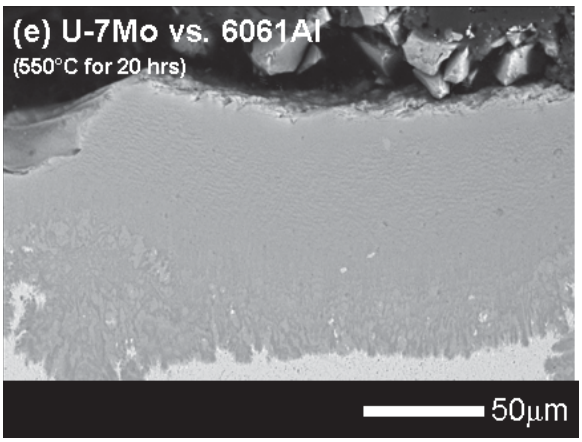

Figure 39. Backscatter electron micrograph of the interdiffusion zone for a U–7Mo vs. Al–6061 diffusion couple annealed at 550°C for 20 hours.

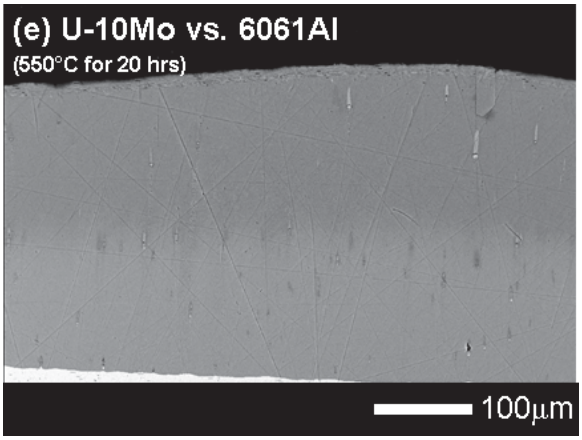

Figure 40. Backscatter electron micrograph of the interdiffusion zone for a U–10Mo vs. Al–6061 diffusion couple annealed at 550°C for 20 hours.

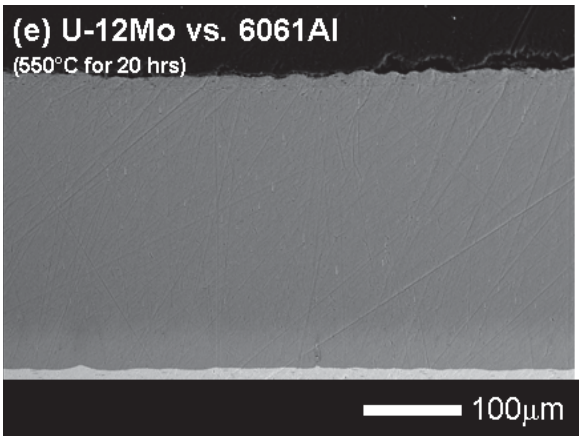

Figure 41. Backscatter electron micrograph of the interdiffusion zone for a U–12Mo vs. Al–6061 diffusion couple annealed at 550°C for 20 hours.

3.3.2.1 More Detailed Microstructural Observations from Couple Treated for 5 Hours

The interdiffusion zone of the U–12Mo vs. Al–6061 was investigated in more detail through EDS standardless compositional analysis and x-ray mapping to assess the re-distribution of elements. Figure 38 shows backscatter electron micrographs of diffusion couple U–12Mo vs. Al–6061 that was annealed at 550°C for 5 hours. This diffusion couple developed a consistent thin interaction zone through the width of the diffusion couple. Areas of greater interactions were observed through the width of the interdiffusion zone. These areas manifested along the length of interdiffusion zone as bumps of varying thickness similar to the one shown in Figure 38(a). Figure 42 shows x-ray maps from this diffusion couple. The reported elements of the Al–6061 alloy, Al, Si, Mg, Ti, Cr, Fe, Cu and Zn, were considered along with U and Mo. With the exception of Si, the trace elements intensities appear too low for reliable measurement. Detailed x-ray maps of the interaction region showing a region of greater interaction and a high magnification region typical of the interdiffusion zone are shown in Figure 43 and Figure 44, respectively. Si appears to accumulate in the interaction region at concentrations larger than the average concentration in the Al–6061 alloy, indicating that diffusion against the Si concentration gradient may be taking place, resulting in the formation of Si-rich phases within the intermetallic region.

The interaction region appears to be divided into a Si-rich region near the UMo/interaction-region interface, and a region that contains some Si near the Al/interaction-region interface. This behavior appears to be typical to the entire interaction region, including the areas of high interaction. EDS semi-quantitative compositional analyses of selected areas of the region are shown in Figure 44. The measured regions are shown in Figure 45, and the compositions are summarized in Table XIV for the major components. Note that due to the size of the interaction region and the nature of the standardless analysis, the measured compositions may contain significant error. Nonetheless, a significant build up of Si can be observed in the interdiffusion zone.

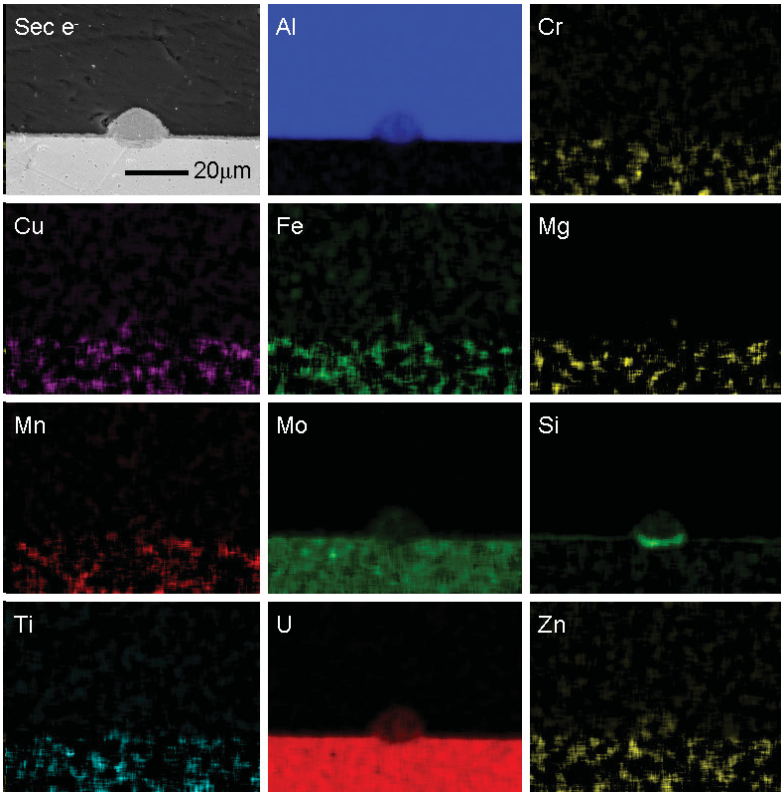

Figure 42. Al, Cr, Cu, Fe, Mg, Mn, Mo, Si, Ti, U, and Zn x-ray maps in the interaction layer of the U–12Mo vs. Al–6061 diffusion couple annealed at 550°C for 5 hours, for a region of low and high interaction.

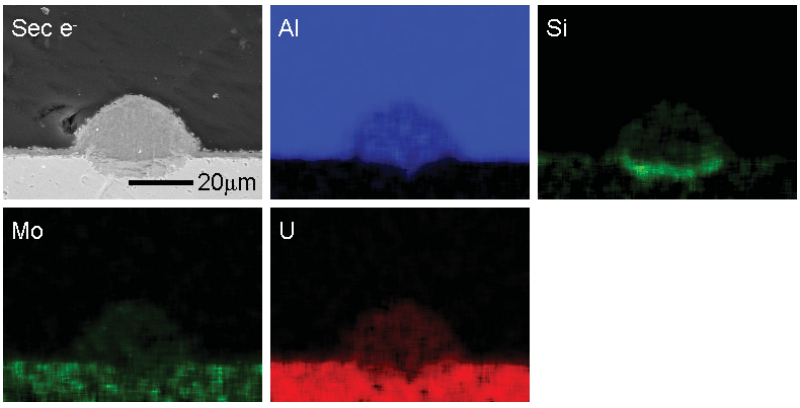

Figure 43. Al, Si, Mo, and U x-rays maps for the interaction layer of a U–12Mo vs. Al–6061 diffusion couple annealed at 550°C for 5 hours in a region of high interaction.

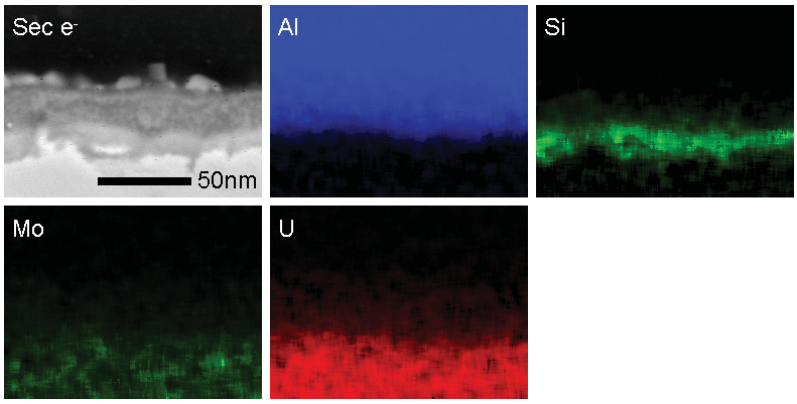

Figure 44. Al, Si, Mo, and U x-rays maps for the interaction layer of a U–12Mo vs. Al–6061 diffusion couple annealed at 550°C for 5 hours, for a typical region.

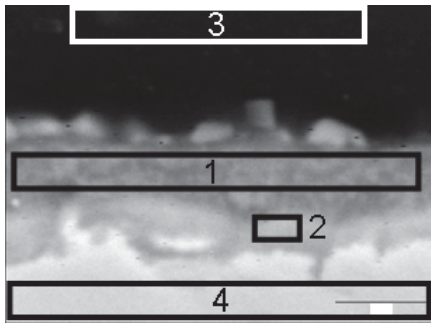

Figure 45. Selected region where compositional analysis was carried out for a diffusion couple annealed at 550°C for 5 hours. The compositions are shown in Table XIV.

Table XIV. EDS Standardless compositional analysis (at.%) of selected regions of the IDZ for a U–12Mo vs. Al–6061 diffusion couple annealed at 550°C for 5 hours.

Element	Area 1	Area 2	Area 3	Area 4
Al	75.8	35.6	97.5	3.0
Si	6.8	24.6	0.1	0.3
Mo	2.9	8.6	0.2	15.4
U	11.5	31.1	0.0	88.9

4. DISCUSSION

4.1 Comparison to Interaction with Pure Al

At temperatures up to 600°C, the diffusion couples in this study exhibited the potential to develop large interaction regions with complex microstructures that contained precipitates with significant compositional differences. The large differences in composition suggest that several phases containing the alloying additions in the commercial Al–6061 developed within the interaction regions. A prior parallel study containing diffusion couples of U–7Mo, U–10Mo, and U–12Mo vs. high purity Al [7, 8] was carried out to determine the phase development in the high purity U–Mo-Al system. As in the current study, diffusion couples of U–Mo vs. pure Al were also annealed at 600°C for 24 hours. Comparison of the developed thicknesses of the diffusion couples with Al–6061 and pure Al shows that the alloying

additions in the Al–6061 alloy may significantly influence the rate of diffusional interactions. Based on the assumption of parabolic growth rate, the diffusion couples containing U–7Mo, U–10Mo, and U–12Mo vs. pure Al had growth constants of 0.90, 1.84, and 1.20 μm/sec^{½}, respectively. The couples with the same U–Mo compositions with Al–6061 had significantly higher growth constants of 2.38, 2.24, and 2.36 μm/sec^{½}. When determining the kinetics of these interactions, the development of liquid phases should be considered, particularly since 600°C is a relatively high temperature in the context of interactions with Al–6061 cladding. As a result, available phase diagrams should be evaluated. In the case of the Al-Si phase diagram, a eutectic exists at 575°C, which means that at a specific binary Al-Si composition (12.2 at% Si-87.8 at% Al), a liquid phase will develop (see Figure 46). At temperatures above 575 up to 600°C, additional combinations of Al and Si concentrations will also be liquid phase. This may help explain the increased kinetics (relative to pure Al) that were observed for the U–Mo couples with Al–6061 cladding annealed at 600°C if one assumes compositions existed in the diffuson zone that became liquid at 600°C. Furthermore, the unique morphology and distribution of phases in the interdiffusion zone, particularly at the cladding side of the interdiffusion zone where higher Si contents were observed, could be due to the presence of liquid phase(s).

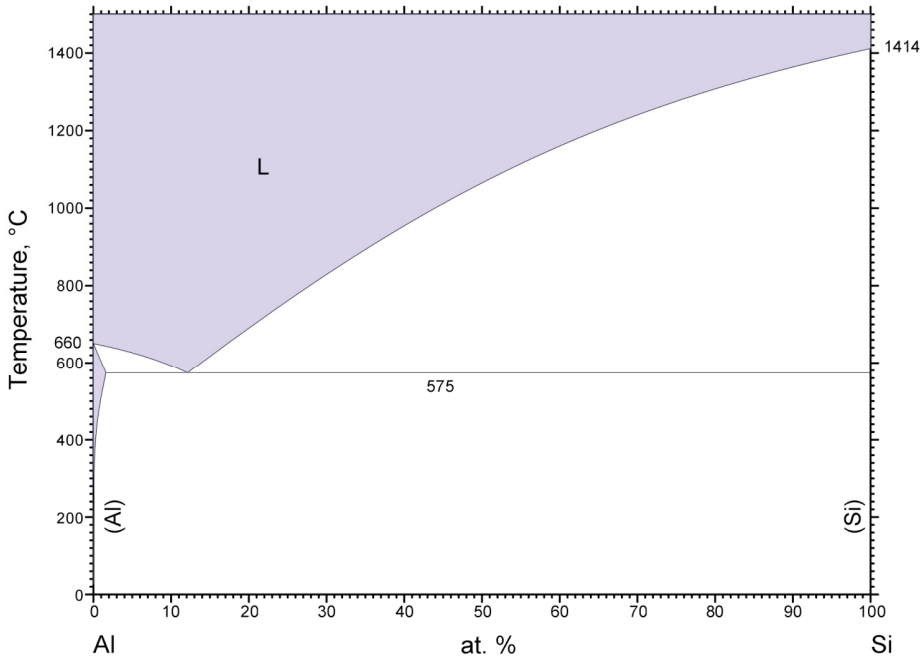

Figure 46. Al-Si Phase Diagram.

For a clearer comparison of the diffusion structures observed for couples with Al and Al–6061 cladding, Figure 47 presents backscatter electron micrographs detailing the microstructural and phase development of the interdiffusion zone in the U–10Mo vs. pure Al diffusion couple annealed at 600°C for 24 hours [7]. A comparison of Figure 29, Figure 30, and Figure 31 with Figure 47 shows some similarities in the microstructural development of the diffusion couples containing Al–6061 and pure Al. Near the center of the interdiffusion zones closer to the U–Mo alloy, the microstructures appear quite similar. Based on the microstructural similarities and the relative contrast in the backscatter electron micrographs, the microstructures of the regions near

the center and closer to the U–Mo alloys in the U–Mo vs. Al–6061 couples may contain similar phase distributions as the diffusion couples with pure Al. The figures also show that significant differences in microstructures are apparent in the interaction regions closer to the Al–6061 and the pure Al. EDS results showed that the development of these regions was strongly affected by diffusion of the alloying additions of the Al–6061.

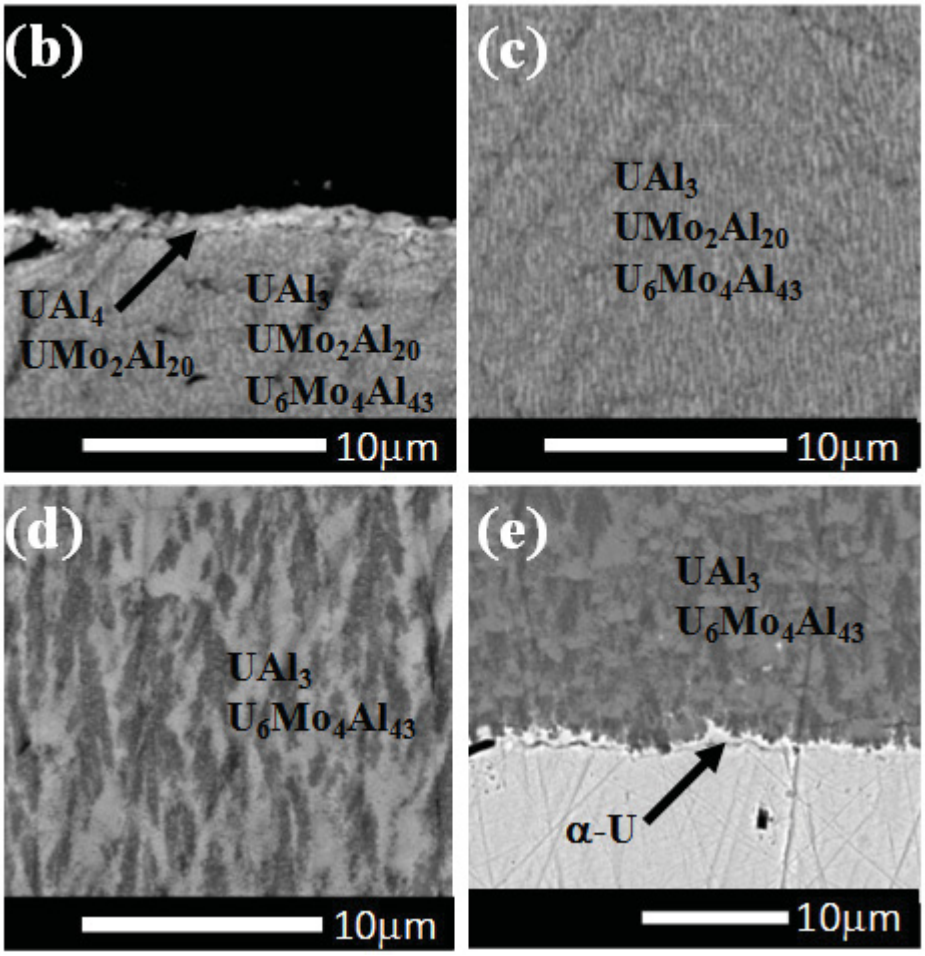

Figure 47. Backscatter electron micrographs detailing the microstructural and phase development of the interdiffusion zone in the U–10Mo vs. pure Al diffusion couple annealed at 600°C for 24 hours [7].

The concentration profile for the U–7Mo vs. Al–6061 diffusion couple, shown in Figure 34, was determined by WDS to identify the average compositional distributions of elements within the interaction region. The profile showed that the Cu, Fe, Mg, and Si alloying additions of the Al–6061 penetrated significantly into the interaction region. Cr was only found very near the interface of the Al–6061 with the interaction region. The profiles show that these alloying additions significantly influenced the Al, Mo, and U concentrations. The Al concentration was significantly reduced where the Cr, Mg, and Si concentrations were high. The U concentration was similarly reduced where the Cu and Fe were observed in measurable concentrations. These results indicate possible solid solubility of the respective elements.

Because the concentration profiles were acquired based on point-to-point analyses, they did not necessarily capture all of the element distributions within the interdiffusion zone. The EDS analysis on discrete precipitates showed that Zn also was also present within the interaction regions. Comparison of the WDS and EDS data tentatively showed that Mn and Ti did not play a role in the evolution of the interaction region, either due to lack of diffusional interactions and/or low concentrations.

In the previous study, concentration profiles were also determined by WDS on the U–Mo vs. pure Al diffusion couples to measure the average concentrations of U, Mo and Al within the interdiffusion zones. Figure 48 shows the typical concentration profile observed in these couples [7]. In that study, the concentration profiles did not develop significant gradients through most of the interdiffusion zone thickness. A comparison of the concentration profile in Figure 34 with Figure 48 shows that the average concentrations of U, Mo, and Al are nearly identical from the center towards the side of the U–Mo alloy in the interaction layer. Aforementioned, the backscatter electron micrographs in Figure 29, Figure 30, and Figure 31 with Figure 34 showed a nearly identical microstructural development. Therefore, the constituent phase development in these regions from the couples with Al–6061 may be similar to that with pure Al where the UAl_3, UAl_4 UMo_2Al_{20}, and $U_6Mo_4Al_{43}$ phases were observed by electron diffraction analysis via transmission electron microscopy [7].

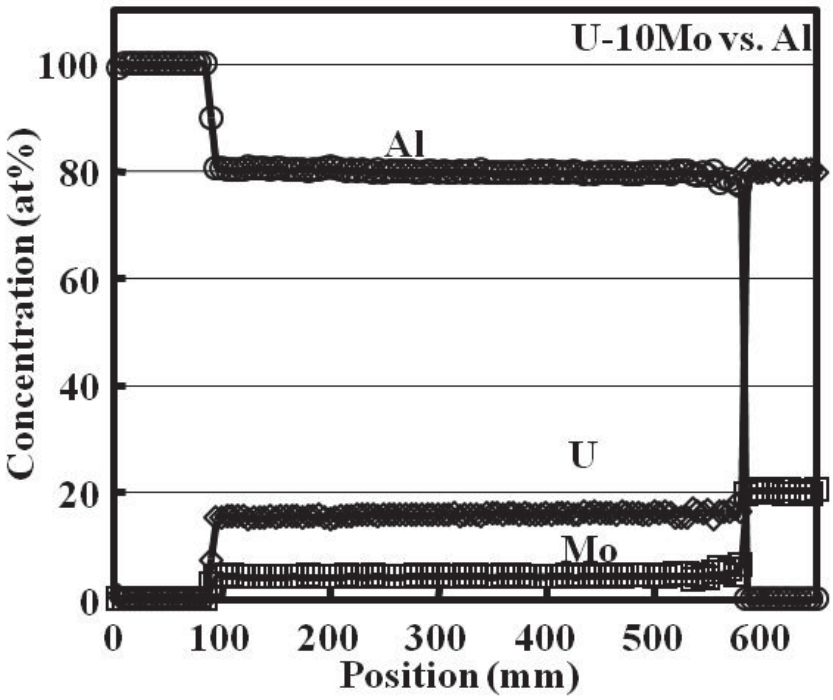

Figure 48. Concentration profile of the U–10Mo vs. Al diffusion couple annealed at 600°C for 24 hours.

Based on a comparison of the results for diffusion experiments using U–Mo alloys and pure Al or Al–6061 cladding annealed at 600°C for 24 hours, the interaction layers for Al–6061 cladding couples can grow at a significantly higher rate than in the case for couples with high-purity Al. These interaction differences should depend on the temperature and time at temperature. Furthermore, the interaction zones for the Al–6061 cladding couples can be more complex in terms of observed phases and morphology of

phase layers. However, there are indications that some similar phases may develop in the interdiffusion zones for both types of couples (e.g., UAl_3, UAl_4 UMo_2Al_{20}, and $U_6Mo_4Al_{43}$).

4.2 Comparison to the Literature

In the literature, results are reported for diffusion couple experiments conducted using U–Mo alloys and Al–6061 cladding, along with other aluminum alloys with many constituents. These experiments were performed using diffusion couples fabricated using a friction bonding technique, instead of solid-solid diffusion couples contained in a Kovar jig. [1, 6, 86]. The potential benefit of a friction bonding process, which uses a rotating tool that impinges into the Al–6061 cladding to promote bonding, is the potential obliteration of any existing oxide layers at the U–Mo/Al–6061 cladding interface, with the result being good bonding at the fuel/cladding interface. Results have also been reported for annealed solid-solid diffusion couples [93].

For diffusion studies using friction-bonded couples, Keiser, Jr. et al. [1] demonstrated that in U–7Mo/Al–6061 and U–10Mo/Al–6061 cladding diffusion couples annealed at 500°C for 0.5 hours both Si- and Al-rich layers can develop in the interdiffusion zone. Larger, non-uniform interaction layers may be observed for couples with U–7Mo alloy vis-à-vis U–10Mo alloy. In general, the largest interaction layers are depleted in Si. For a relatively long heat treatment of 100 hours at 500°C, a 250-μm-thick U–10Mo foil can be completely consumed, leaving behind a mutliphase layer enriched in Al. Mirandou et al. [86] demonstrated that in U–7Mo/Al–6061 couples annealed at 550°C for up to 3 hours irregular interdiffusion layers develop that vary in thickness from 6 to 300 μm. A thin band is generallly observed with up to 17 at.% Si, but irregular localized regions, up to 300-μm-thick, can also develop that contain negligible Si. Micro- XRD analysis was performed using synchrotron radiation (at the Brazilian Synchrotron Light Laboratory) to identify phases present in the layers. It was determined that UAl_3 and $U_6Mo_4Al_{43}$ were the primary phases present in the thicker regions, and these regions were generally located near areas in the U–7Mo where γ-(U,Mo) phase had decomposed to α-U and γ' (U_2Mo). The thin, Si-rich interaction layer contained $U(Al,Si)_3$ as the primary phase, and it was generally observed near the U–7Mo where γ-(U,Mo) phase had remained stable. In couples annealed at 340°C, a U_3Si_5 could be found in the interdiffusion zone. With regard to a precipitate-free zone (PFZ) that is commonly found in the Al alloy near the interaction zone for annealed U–Mo vs. Al-Si alloy diffusion couples, Mirandou observed one at 340°C, but not at 550°C. This was supposedly due to the fact that since 550°C is higher than the 529°C solution temperature for Al 6061 alloy, precipitates should dissolve and then re-precipitate during cooling resulting in no observable PFZ. For another diffusion study performed by Mirandou et al. [6], $U(Al,Si)_3$ (with 35 at.% Si), UMo_2Al_{20}, and U_3Si_5 were identified when using synchrotoron XRD analysis to characterize the interaction layers that developed in diffusion couples between U–7Mo and AA356 alloy (7.1 wt.% Si) that were annealed at 550°C. For couples annealed at 340°C, $U(Al,Si)_3$ and U_3Si_5 were observed.

In [93], results for solid-solid U–7Mo/Al–6061 couples annealed for 2 hours at 580°C have been reported. The couples were anealed as part of assemblies where polished U–7Mo alloy was inserted between a polished piece of pure Al and a polished piece of Al–6061 cladding. For the U–7Mo versus Al–6061 cladding couple, the interdiffusion zone had a composition, in at.%, of approximately 20U-2Mo-(2-3)Si-(75-76)Al. The overall interdiffusion zone was 129 μm thick. The interdiffusion zone that formed between the U–7Mo and pure Al was 150 μm thick.

The following are literature observations that agree with what has been observed for U–Mo alloy versus Al–6061 cladding diffusion couples annealed as part of the current investigation: (1) non-uniform interaction layers develop that are comprised of Si- and Al-rich phases, (2) complex microstructures are observed in the interaction layers, (3) interaction layers exhibit relatively high growth kinetics, and (4) some phases in the interaction layers are similar to those that form in couples with pure Al.

5. CONCLUSIONS

Based on the results of solid-solid diffusion couple experiments performed at 500, 550, and 600°C using U-xMo (x=7, 10, 12) alloys and Al–6061 cladding, the following conclusions can be drawn: (1) the presence of surface layers at the U–Mo/Al–6061 interface can dramatically impact the overall interdiffusion behavior in terms of rate of interaction and uniformity of the developed interdiffusion zones; (2) relatively uniform interaction layers with higher Si concentrations can develop in U–Mo/Al–6061 couples annealed at shorter times; (3) longer times at temperature result in the development of more non-uniform interaction layers with more areas that are enriched in Al; (4) at longer annealing times and relatively high temperatures, U–Mo/Al–6061 couples can exhibit more interaction compared to U–Mo/pure Al couples; (5) the minor alloying constituents in Al–6061 cladding can result in the development of many complex phases in the interaction layer of U–Mo/Al–6061 cladding couples, and (6) some phases in the interdiffusion zones of U–Mo/Al–6061 cladding couples are likely similar to those observed for U–Mo/pure Al couples.

6. REFERENCES

[1] D.D. Keiser Jr.: *Def. Diffus.*, 2007, vol. 266, pp. 131-48.

[2] E. Perez, N. Hotaling, A. Ewh, D.D. Keiser and Y. H. Sohn: *Def. Diffus.*, 2007, vol. 266, pp. 149-56.

[3] M.I. Mirandou, S. Balart, M. Ortiz and M.S. Granovsky; *J. Nucl. Mater.*, 2003, vol. 323, pp. 29-35.

[4] H. Palancher. P. Martin, V. Nassif, R. Tucoulou, O. Proux, J.-L.- Hazemann, O. Tougait, E. Lahéra, F. Mazaudier, C. Valot and S. Dubois: *J. Appl. Crystallogr.*, 2007, vol. 40, pp. 1064-75.

[5] F. Mazaudier, C. Proye and F. Hodaj: *J. Nucl. Mater.*, 2008, vol. 377, pp. 476-85.

[6] M.I. Mirandou, S.F. Arico, S.N. Balart and L.M. Gribaudo: *Mater. Charact.*, 2009, vol. 60, pp. 888-93.

[7] E. Perez, D.D. Keiser Jr. and Y.H. Sohn: *Metall. Mater. Trans. A*, 2011, vol. 42A, pp. 3071-83.

[8] E. Perez, D.D. Keiser and Y.H. Sohn: *Def. Diffus. Forum*, 2009, vols. 289-92, pp. 41-49.

[9] D.D. Keiser Jr., C.R. Clark and M.K. Meyer: *Scr. Mater.*, 2004, vol. 51, pp. 893-98.

[10] E. Perez, A. Ewh, J. Liu, B. Yuan, D.D. Keiser Jr. and Y.H. Sohn: *J. Nucl. Mater.*, 2009, vol. 394, pp. 160-65.

[11] D.B. Lee, K.H. Kim and C.K. Kim: *J. Nucl. Mater.*, 1997, vol. 250, pp. 79-82.

[12] K.H. Kim, D.B. Lee, C.K. Kim, G.L. Hofman and K.W. Paik: *Nucl. Eng. Des.*, 1997, vol. 178, pp. 111-17.

[13] D.D. Keiser Jr, S.L. Hayes, M.K. Meyer and C.R. Clark: *JOM*, 2003, vol. 55, no. 9, pp. 55-58.

[14] S.H. Lee, J.C. Kim, J.M. Park, C.K. Kim and S.W. Kim: *Int. J. Thermophys.*, 2003, vol. 24, no. 5, pp. 1355-71.

[15] S.H. Lee, J.M. Park and C.K. Kim: *Int. J. Thermophys.*, 2007, vol.28, no.5, pp. 1578-94.

[16] J.-S. Lee, C.-H. Lee, K. H. Kim and V. Em: *J. Nucl. Mater.*, 2002, vol. 306, pp. 147-52.

[17] H.J. Ryu, Y.S. Han, J.M. Park, S.D. Park and C.K. Kim, *J. Nucl. Mater.*, 2003, vol. 321 pp. 210-20.

[18] H.J. Ryu, J.M. Park, C.K. Kim and G.L. Hofman: *J. Phase Equilib. and Diffus.*, 2006, vol. 27, no. 6, pp. 651-58.

[19] H. Etherington, *Nuclear Engineering Handbook*, McGraw Hill Book Co., New York, NY, 1958, pp. 12.54 – 12.55.

[20] *Federal Register, Rules and Regulations*, vol. 51, no. 37, Feb. 25, 1986.

[21] J.L. Snelgrove, G.L. Hofman, M.K. Meyer, C.L. Trybus and T.C. Wiencek: *Nucl. Eng. Des.*, 1997, vol. 178, pp. 119-26.

[22] P.C.L. Pfeil: *J. Inst. Met.*, 1950, vol. 77, pp. 553-70.

[23] H.A. Saller, F.A. Rough and D.A. Vaughan: *U.S.A.E.C.*, BMI-72, 1951.

[24] H.A. Saller, F.A. Rough and D.C. Bennet: *U.S.A.E.C.*, BMI-730, 1952.

[25] H.A. Saller and F.A. Rough: *U.S.A.E.C.*, BMI-752, 1952.

[26] A.J. Carrea, D.R.F. West and J.G. Ball: *J. Nucl. Energy*, 1958, vol. 7, pp. 189-98.

[27] A.E. Dwight: *J. Nucl. Mater.*, 1960, vol. 2, no. 1, pp. 81-87.

[28] K. Tangri and G.I. Williams: *J. Nucl. Mater.*, 1961, vol. 4, no. 2, pp. 226-33.

[29] O.S. Ivanov and Y.S. Virgiliev: *J. Nucl. Mater.*, 1962, vol. 6, no. 2, pp. 199-202.

[30] G.H. May: *J. Nucl. Mater.*, 1962, vol. 7, no.1, pp. 72-84.

[31] C.G. Rhodes and D. Kramer: *J. Nucl. Mater.*, 1963, vol. 9, no.1, pp. 114-15.

[32] A. Mihajlović, M. Kostić and P. Tepavac: *J. Nucl. Mater.*, 1969, vol. 31, pp. 107-10.

[33] J.G. Speer and D.V. Edmonds, *Acta Metall.*, 1988, vol.36, no. 4, pp. 1015-33.

[34] O.S. Ivanov, T.A. Badaeva, R.M. Sofronova, V.B. Kishenevshii, N.P. Kushnir, and O.S. Ivanov: *Phase Diagrams of Uranium Alloys*, Amerind Publishing Co. Pvt. Ltd., New Delhi, India, 1983, pp. 29-33.

[35] L.B. Lundberg: *J. Nucl. Mater.*, 1989, vol. 167, pp. 64-75.

[36] K.H. Kim, D.B. Lee, C.K. Kim and G.E. Hofman: *J. Nucl. Mater.*, 1997, vol. 245, pp. 179-84.

[37] B.-S. Seong, C.H. Lee, J.-S. Lee, H.-S. Shim, J.-H. Lee, K.H. Kim, C.K. Kim and V. Em: *J. Nucl. Mater.*, 2000, vol. 277, pp. 274-79.

[38] J.-S. Lee, C.-H. Lee, K.H. Kim and V. Em: *J. Nucl. Mater.*, 2000, vol. 280, pp. 116-19.

[39] A.V. Vatulin, A.V. Morozov, V.B. Suprun, Y.I. Petrov and Y.I. Trifonov: *Met. Sci. Heat Treat.*, 2004, vol. 46, nos. 11-12, pp. 484-89.

[40] V.P. Sinha, G.J. Prasad, P.V. Hedge, R. Keswani, C.B. Basak, S. Pal and G.P. Mishra: *J. Alloys Compd.*, 2009, vol. 473, pp. 238-44.

[41] J.M. Park, H.J. Ryu, K.H. Kim, D.B. Lee, Y.S. Lee, J.S. Lee, B.S. Seong, C.K. Kim and M.Coren: *J. Nucl. Mater.*, 2010, vol. 397, pp. 27-30.

[42] M. Chen, Y.-F. Xiong, W.-Y. Jing, J.-P. Jia and P.-C. Zhang, *J. Nucl. Mater.*, 2010, vol. 400, pp. 69-72 .

[43] V.P. Sinha, P.V. Hegde, G.J. Prasad, G.K. Dey and H.S. Kamath: *J. Alloys Compd.*, 2010, vol. 491, pp. 753-60.

[44] V.P. Sinha, P.V. Hegde, G.J. Prasad, G.K. Dey and H.S. Kamath, *J. Alloys Compd.*, 2010, vol. 506, pp. 253-62.

[45] H.A. Saller, F.A. Rough and A.A. Bauer: *U.S.A.E.C.*, BMI-957, 1954.

[46] R.F. Hills, B.R. Butcher and J.A. Heywood: *J. Less-Common Met.*, 1961, vol. 3, pp. 155-69.

[47] R.F. Hills, B.W. Howlet and B.R. Butcher: *J. Less-Common Met.*, 1963, vol. 5, pp. 369-73.

[48] B.W Howlett, A.J. Eycott, I.K. Kang and D.R.F. West: *J. Nucl. Mater.*, 1963, vol. 9, no.2, pp. 143-54.

[49] G. Östberg, M. Möller and B. Schönning-Cristiansson, *J. Nucl. Mater.*, 1963, vol. 10, no. 4, pp. 329-38.

[50] P.E. Repas, R.H. Goodenow and R.F. Hehemann; *Trans. ASM*, 1964, vol. 57, pp. 150-63.

[51] G. Östberg and B. Lehtinen: *J. Nucl. Mater.*, 1964, vol. 13, no.1, pp. 123-24.

[52] Y. Goldstein and A. Bar-Or: *J. Inst. Met.*, 1967, vol. 95, pp. 17-21.

[53] R.F. Hills, B.R. Butcher and B.W. Howlett: *J. Nucl. Mater.*, 1964, vol. 11, no. 2 pp. 149-62.

[54] B.R. Butcher and B.A. Hatt: *J. Nucl. Mater.*, 1964, vol. 11, no.2, pp. 163-82.

[55] D.E. Burkes, T. Hartmann, R. Prabhakaran and J.-F. Jue: *J. Alloys Compd.*, 2009, vol. 479, pp. 140-47.

[56] D.E. Burkes, R. Prabhakaran, T. Hartmann, J.-F. Jue and F. J. Rice: *Nucl. Eng. Des.*, 2010, vol. 240, pp. 1332-39.

[57] D.E. Burkes, C.A. Papesch, A.P. Maddison, T. Hartmann and F.J. Rice, *J. Nucl. Mater.*, 2010, vol. 403, pp. 160-66.

[58] F.J. Blatt: *J. Phys. Chem. Solids*, 1961. vol. 17, nos. 3-4, pp. 177-87.

[59] Y.V. Vamberskiy, A.L. Udovskiy and O.S. Ivanov: *J. Nucl. Mater.*, 1973, vol. 46, pp. 192-206.

[60] T. Matsui, T. Natsume and K. Naito: *J. Nucl. Mater.*, 1989, vol. 167, pp. 152-59.

[61] S.C. Parida, S. Dash, Z. Singh, R. Prasad and V. Venugopal: *J. Phys. Chem. Solids*, 2001, vol. 62, pp. 585-97.

[62] R.M. Hengstler, L. Beck, H. Breitkreutz, C. Jarousse, R. Jungwirth, W. Petry, W. Schmid, J. Schneider and N. Wieschalla: *J. Nucl. Mater.*, 2010, vol. 402, pp. 74-80.

[63] M.L. Bleiberg, L.J. Jones and B. Lustman: *J. Appl. Phys.*, 1956, vol. 27, no. 11, pp. 1270-83.

[64] S.T. Konobeevsky: *J. Nucl. Energy*, 1956, vol. 3, pp. 356-65.

[65] M.L. Bleiberg: *J. Nucl. Mater.*, 1959, vol. 2, pp. 182-90.

[66] S.T. Konobeevsky, N.F. Pravdyuk, K.P. Dubrovin, B.M. Levitskii, L.D. Panteleev and V.M. Golianov: *J. Nucl. Energy II*, 1959, vol. 9, pp. 75-89.

[67] M.K. Meyer, G.L. Hofman, S.L. Hayes, C.R. Clark, T.C. Wiencek, J.L. Snelgrove, R.V. Strain and K.-H. Kim: *J. Nucl. Mater.*, 2002, vol. 304, pp. 221-36.

[68] K.H. Kim, J.-M. Park, C.-K. Kim, G.L. Hofman and M.K. Meyer: *Nucl. Eng. Des.*, 2002, vol. 211, pp. 229-35.

[69] A. Leenaers, S. Van den Berghe, E. Koonen, C. Jarousse, F. Huet, M. Trotabas, M. Boyard, S. Guillot, L. Sannen and M. Verwerft: *J. Nucl. Mater.*, 2004, vol. 335, pp. 39-47.

[70] A.V. Vatulin, A.V. Morozov, V.B. Suprun, Y.I. Petrov and Y.I. Trifonov: *At. Energy*, 2006, vol. 100, no.1, pp. 37-46.

[71] S. Van den Berghe, W.V. Renterghem and A. Leenaers: *J. Nucl. Mater.*, 2008, vol. 375, pp. 340-46.

[72] J. Rest, G.L. Hofman and Y.S. Kim: *J. Nucl. Mater.*, 2009, vol.385, pp. 563-71.

[73] D.D. Keiser Jr., A.B. Robinson, J.-F. Jue, P. Medvedev, D.M. Wachs and M.R. Finlay: *J. Nucl. Mater.*, 2009, vol. 393, pp. 311-20.

[74] L.I. Gomozov, E.M. Lyutina and O.S. Ivanov: *Izv. Akad. Nauk SSSR, Metal.*, 1970, no.2, pp. 210-15.

[75] Y.S. Kim, G.L. Hofman, H.J. Ryu and S.L. Hayes: *J. Phase Equilib. Diffus.*, 2006, vol. 27, no.6, pp. 614-21.

[76] N. Wieschalla, A. Bergmaier, P. Böni, K. Böning, G. Dollinger, R. Groβmann, W. Petry, A. Röhrmoser and J. Schneider: *J. Nucl. Mater.*, 2006, vol. 357, pp. 191-97.

[77] H.J. Ryu, Y.S. Kim, J.M. Park, H.T. Chae and C.K. Kim: *Nucl. Eng. Technol.*, 2008, vol. 40, no.5, pp. 409-18.

[78] H. Palancher, N. Wieschalla, P. Martin, R. Tucoulou, C. Sabathier, W. Petry, J.-F. Berar, C. Valot and S. Dubois: *J. Nucl. Mater.*, 2009, vol. 385 pp. 449-55.

[79] H.J. Ryu, Y.S. Kim and G.L. Hofman: *J. Nucl. Mater.*, 2009, vol. 385, pp. 623-28.

[80] M.Rodier, X.Iltis, F.Mazaudier, M. Cornen, S.Dubois, Transactions of the 11th International Topical Meeting on Research Reactor Fuel Management and Meeting of the International Group of Reactor Research, Centre de Congrès, Lyon, France, March 11-15, 2007.

[81] M.A. Dayananda and C.W. Kim, Zero-Flux Planes and Flux Reversals in Cu-Ni-Zn Diffusion Couples, Metall. Trans. A, 1979, 10A, p 1333-1339.

[82] E. Perez, B. Yao, Y.H. Sohn and D.D. Keiser Jr.: *Proc. Int. Meet. Reduced Enrich. Res. Test React.*, Nov. 1-5, 2009, Beijing, China.

[83] J.M. Park, H.J. Ryu, S.J. Oh, D.B. Lee, C.K. Kim, Y.S. Kim and G.L. Hofman: *J. Nucl. Mater.*, 2008, vol. 374, pp. 422-30.

[84] C.K. Varela, M. Mirandou, A. Aricó, S. Balart and L. Gribaudo: *J. Nucl. Mater.*, 2009, vol 395, pp. 162-68.

[85] J. Gan, D.D. Keiser Jr., D.M. Wachs, A.B. Robinson, B.D. Miller and T.R. Allen: *J. Nucl. Mater.*, 2010, vol. 396, pp. 234-39.

[86] M. Mirandou, S. Aricó, M. Rosenbusch, M. Ortiz, S. Balart and L. Gribaudo: *J. Nucl. Mater.*, 2009, vol. 384, pp. 268-73.

[87] D.D. Keiser Jr., J. Gan, J.F. Jue, B.D. Miller and C.R. Clark: *Mater. Charact.*, 2010, vol. 61, pp. 1157-66.

[88] D.R. Green: *U.S.A.E.C.*, HW-49697, 1957.

[89] A.E. Dwight: Argonne Natl. Lab., ANL-82-14, UC-25, 1982.

[90] C.-K. Rhee, S.-I. Pyun and I.-H. Kuk: *J. Nucl. Mater.*, 1991, vol. 184, pp. 161-66.

[91] K.H. Kim, J.M. Park, C.K. Kim, G.L. Hofman and K.-W. Paik: *J. Nucl. Mater.*, 1999, vol. 270, pp. 315-21.

[92] E. Perez, Y.H. Sohn, D.D. Keiser, Jr.: *Metall. Mater. Trans. A*, 2013, vol. 44A, pp. 584-95.

[93] M. Mirandou, M. Granovsky, M. Ortiz, S. Balart, S. Arico, and L. Gribaudo, "Reaction Layer Between U-7 wt% Mo and Al Alloys in Chemical Diffusion Couple," in: *Proceedings of the 26th International Meeting on Reduced Enrichment for Research and Test Reactors (RERTR)*, Vienna, Austria, Nov. 7-12, 2004.